

# **Laboratory Evaluation of Gap Graded Asphalt Concrete Mixtures – Malmo E6 External Ring Road, Sweden**

Final Report

Prepared by

**Kamil E. Kaloush, Ph.D., P.E.**  
Associate Professor

**Krishna P. Biligiri**  
**Waleed A. Zeiada**  
**Maria Carolina Rodezno**  
**Mena I. Souliman**  
Graduate Research Associates

Submitted to  
**Mr. Thorsten Nordgren**  
**Swedish Road Administration**  
Vägverket  
405 33 Göteborg  
Kruthusgatan 17, Sweden

October 2008



**Ira A. Fulton School of Engineering**  
**Department of Civil and Environmental Engineering**  
Tempe, AZ 85287-5306

## TABLE OF CONTENTS

	Page
LIST OF TABLES .....	2
LIST OF FIGURES .....	3
1. INTRODUCTION .....	4
1.1. Study Objectives .....	4
1.2. Scope of the Work .....	4
1.3. Number of Tests.....	7
1.4. Report Organization.....	7
2. MIXTURE CHARACTERISTICS .....	9
3. DYNAMIC COMPLEX MODULUS TEST .....	10
3.1. Introduction.....	10
3.2. Master Curve.....	13
3.3. Summary of Test Method .....	14
3.4. Test Results .....	17
3.5. Mixtures Comparison.....	22
4. REPEATED LOAD PERMANENT DEFORMATION TESTS.....	26
4.1. Background for the Repeated Load Permanent Deformation Test .....	26
4.2. Test Conditions for the Repeated Load Tests .....	27
4.3. Repeated Load / Flow Number Test Results and Analysis.....	28
5.FATIGUE CRACKING TESTS.....	30
5.1. Background of the Flexural Beam Fatigue Test .....	30
5.2. Testing Equipment .....	32
5.3. Test Procedure and Calculations.....	33
5.4. Materials and Specimen Preparation .....	35
5.5. Testing Factorial .....	39
5.6. Test Results and Analysis .....	40
6. CRACK PROPAGATION TEST – C* LINE INTEGRAL .....	43
6.1. Background .....	43
6.2. C* Parameters .....	44
6.3. Test Specimen and Test Conditions.....	45
6.4. Method for C* Determination.....	47
7. TIRE / ROAD NOISE LABORATORY EVALUATION .....	54
7.1. Phase Angle Test Results.....	55
7.2. Phase Angle Master Curve.....	56
8. SUMMARY AND CONCLUSIONS .....	58
8.1. Summary .....	58
8.2. Conclusions.....	58
REFERENCES .....	61

## LIST OF TABLES

	Page
Table 1 Mixture Characteristics, Swedish Malmo E6 External Ring Road. ....	9
Table 2 Average Aggregate Gradations, Malmo E6 External Ring Road. ....	9
Table 3 Test Conditions of the Dynamic Modulus (E*) Test.....	15
Table 4 Summary of E* and Phase Angle values for Unconfined Reference Gap Graded Mix. ....	18
Table 5 Summary of E* and Phase Angle values for Unconfined Asphalt Rubber Gap Graded Mix. ....	19
Table 6 Comparison of Modular Ratios (R). ....	23
Table 7 Master Summary of Repeated Load Test Results, Swedish Malmo E6 Mixtures. .....	28
Table 8 Control Strain Beam Fatigue Test Results for the Reference Gap Graded Mixture. .....	41
Table 9 Control Strain Beam Fatigue Test Results for the Asphalt Rubber Gap Graded Mixture.....	41
Table 10 Summary of Regression Coefficients for the Fatigue Relationships at 50% of Initial Stiffness, Swedish Mixtures, 21.1 °C.....	41
Table 11 Displacement Rates Used for Both Mixtures. ....	47
Table 12 Summary of Test Results for the Reference Gap Mix. ....	50
Table 13 Summary of Test Results for the Asphalt Rubber Gap Mix.....	51
Table 14 Phase Angle Test Results of Swedish Gap Graded Mixtures.....	55
Table 15 Relationship between Phase Angle and Field Noise for Different Vehicle Speeds .....	57

## LIST OF FIGURES

	Page
Figure 1 Location of Malmo E6 External Ring Road, Sweden. ....	6
Figure 2 Crumb Rubber Granular. ....	6
Figure 3 Compacted Gyrotory Plugs.....	7
Figure 4 Stress-Strain Cycle, Dynamic Modulus Test.....	11
Figure 5 Specimen Instrumentation of E* Testing. ....	16
Figure 6 Malmo E6 External Ring Road Gap Graded Samples. ....	16
Figure 7 Typical E* Test Sample.....	16
Figure 8 Reference Gap Graded Mix (a) Master Curve based on Average of Three Replicates (b) Shift Factors based on Average of Three Replicates (c) Master Curve of a Typical Replicate. ....	20
Figure 9 Asphalt Rubber Gap Graded Mix (a) Master Curve based on Average of Three Replicates (b) Shift Factors based on Average of Three Replicates (c) Master Curve of a Typical Replicate. ....	21
Figure 10 Comparison of E* Master Curves. ....	22
Figure 11 Comparison of Measured Dynamic Modulus E* values at 4.4 °C for the Reference and the Asphalt Rubber Gap Graded Mixtures at 10 and 0.5 Hz .....	24
Figure 12 Comparison of Measured Dynamic Modulus E* values at 37.8 °C for the Reference and Asphalt Rubber Gap Graded Mixtures at 10 and 0.5 Hz .....	25
Figure 13 Typical Relationship between Total Cumulative Plastic Strain and Number of Load Cycles .....	26
Figure 14 Vertical and Radial LVDTs Set Up for an Unconfined Test.....	27
Figure 15 Repeated Load Permanent Deformation Flow Number Test Results, Swedish Malmo E6 Gap Graded Mixtures.....	29
Figure 16 Flexural Fatigue Apparatus .....	32
Figure 17 Loading Characteristics of the Flexural Fatigue Apparatus .....	33
Figure 18 Manufactured Mold for Beam Compaction .....	37
Figure 19 Top Loading Platen .....	37
Figure 20 Beam specimen sawing. ....	38
Figure 21 Typical Reference and Asphalt Rubber Beams. (Photos taken after test).....	39
Figure 22 Comparison of Fatigue Relationships at 50% of Initial Stiffness. ....	42
Figure 23 Comparison of Fatigue Relationships at 30% of Initial Stiffness. ....	42
Figure 24 C* Integral Test Results for Several Modified Asphalt Mixtures (16). ....	45
Figure 25 Typical C* Test Setup .....	46
Figure 26 Typical C* Test Samples.....	47
Figure 27 Method of Area Calculations.....	49
Figure 28 Crack Lengths versus Energy Rate for the Reference Gap Mix. ....	52
Figure 29 Crack Lengths versus Energy Rate for Asphalt Rubber Gap Mix. ....	52
Figure 30 Crack Growth Rate versus C* Values For Reference and Rubber Gap Mixes. ....	53
Figure 31 Asphalt Mixture Stress-Strain Responses under Sinusoidal Load for Different Levels of Viscoelastic Behavior .....	54
Figure 32 Phase Angle Master Curves for the Reference and Asphalt Rubber Gap Graded Mixtures. ....	57

## **1. INTRODUCTION**

### **1.1. Study Objectives**

The objective of this study was to conduct a laboratory experimental program to obtain material properties and performance characteristics for a “Reference Gap” and “Asphalt Rubber (AR) Gap” graded mixtures that were used on the Swedish Malmo E6 External Ring Road.

### **1.2. Scope of the Work**

Both the reference and asphalt rubber gap graded mixtures were sampled by the Swedish Road Administration from pavement sections constructed on Malmo E6 External Ring Road. The mixtures were transported to Arizona State University (ASU) laboratories, where they were re-heated and compacted to cylindrical and beam specimen geometry. A Servopac gyratory compactor was used to compact the cylindrical specimens into 150 mm diameter and 170 mm in height gyratory plugs. One 100 mm diameter sample was cored from each gyratory plug. The sample ends were sawn to arrive at typical test specimens of 100 mm in diameter and 150 mm in height. Beam specimens were prepared according to the Strategic Highway Research Program (SHRP) and the American Association of State Highway and Transportation Officials (AASHTO): SHRP M-009 (1) and AASHTO TP8-94 (2), and. In addition, disc specimens saw cut from gyratory plugs (150 mm in diameter and approximately 40 mm thick) were prepared according to the “Test Method for Indirect Tensile Creep Testing of Asphalt Mixtures for Thermal Cracking” reported in NCHRP Report 465 (3). Air voids, thickness and bulk specific

gravities were measured for each test specimen and the samples were stored in plastic bags in preparation for the testing program.

The designated road section within the construction project had two asphalt mixtures: a reference gap graded mix used as a control, and an asphalt rubber mixture that contained approximately 20 percent ground tire rubber (crumb rubber). Figure 1 shows a map of Malmo E6 External Ring Road where the two mixtures were placed. Figure 2 is an illustration of the crumb rubber granular that were used in the modification of the virgin binder for the AR gap graded mix. Figure 3 shows typical compacted gyratory samples.

The advanced material characterization tests included: Dynamic (Complex) Modulus for stiffness evaluation, beam fatigue cracking evaluation, and C\* Integral test to evaluate crack propagation.

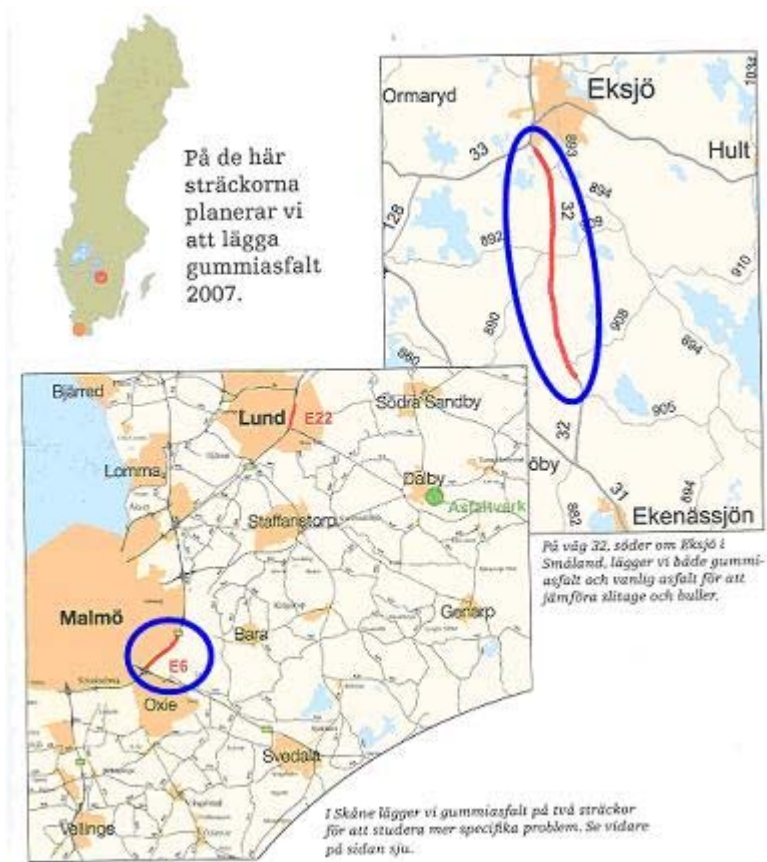


Figure 1 Location of Malmo E6 External Ring Road, Sweden.



Figure 2 Crumb Rubber Granular.



Figure 3 Compacted Gyratory Plugs.

### 1.3. Number of Tests

Below is the number of tests conducted for each mixture:

- Dynamic Complex Modulus  
Unconfined x 5 temperatures x 6 frequencies x 3 replicates = 90 tests
- Repeated Load Permanent Deformation Flow Number  
Unconfined x 1 temperature (30 °C) x 3 replicates = 3 tests
- Beam Fatigue  
1 temperature (21.1 °C) x 4 strain levels = 4 tests
- C\* Integral Test  
1 temperature (21.1 °C) x 5 displacement rates = 5 tests

### 1.4. Report Organization

This report is divided into seven sections. Section 1 included the study objective and scope of work. Section 2 summarizes the mixture properties. Section 3 documents the Dynamic Modulus tests; Section 4 includes repeated load permanent deformation flow number tests; whereas Section 5 includes the beam fatigue test results. Section 6 contains the C\* Integral crack propagation test results. Section 7 discusses the phase angle test

results and laboratory indication of tire / pavement noise characteristics. Section 8 presents the summary, conclusions and recommendations of the study.

## 2. MIXTURE CHARACTERISTICS

This section provides some details on the materials used and the mixtures' characteristics.

The Swedish Road Administration provided information stating that the field compaction / air voids for both the mixtures was 2.0%. The original mix designs were done using the Marshall Mix design method. The in-situ mixture properties of the Swedish Highway E-06 project are reported in Table 1. Table 2 shows the reported average aggregate gradations for the each mixture. The base bitumen used was Pen 70/100.

Table 1 Mixture Characteristics, Swedish Malmo E6 External Ring Road.

Mix	Bitumen Content (%)	Air Voids (%)	G <sub>mb</sub>	G <sub>mm</sub>
Reference Gap Graded	6.0	2	2.406	2.453
AR - Gap Graded	6.7	2	2.348	2.396

Table 2 Average Aggregate Gradations, Malmo E6 External Ring Road.

Gradation (% Passing)	Sieve Size (mm)	Ref Gap Graded	AR-Gap Graded
	63	100	100
	50	100	100
	45	100	100
	31.5	100	100
	22.4	100	100
	16	94	98
	11.2	54	66
	8	36	43
	5.6	29	30
	4	24	23
	2	22	21
	1	20	16
	0.5	18	13
	0.25	16	10
	0.125	12	7
	0.063	9.8	4.6

### 3. DYNAMIC COMPLEX MODULUS TEST

#### 3.1. Introduction

The Dynamic Modulus ( $E^*$ ) laboratory test is one of the major input material properties for flexible pavement design. It has been recommended as a Simple Performance Test (SPT) under the National Cooperative Highway Research Program (NCHRP) Project 9-19 (3).

For linear viscoelastic materials such as asphalt mixtures, the stress-to-strain relationship under a continuous sinusoidal loading is defined by its complex dynamic modulus ( $E^*$ ). This is a complex number that relates stress to strain for linear viscoelastic materials subjected to continuously applied sinusoidal loading in the frequency domain. The complex modulus is defined as the ratio of the amplitude of the sinusoidal stress (at any given time,  $t$ , and angular load frequency,  $\omega$ ),  $\sigma = \sigma_0 \sin(\omega t)$  and the amplitude of the sinusoidal strain  $\varepsilon = \varepsilon_0 \sin(\omega t - \phi)$ , at the same time and frequency, that results in a steady state response (Figure 4):

$$E^* = \frac{\sigma}{\varepsilon} = \frac{\sigma_0 e^{i\omega t}}{\varepsilon_0 e^{i(\omega t - \phi)}} = \frac{\sigma_0 \sin \omega t}{\varepsilon_0 \sin(\omega t - \phi)}$$

Where,

$\sigma_0$  = peak (maximum) stress

$\varepsilon_0$  = peak (maximum) strain

$\phi$  = phase angle, degrees

$\omega$  = angular velocity

$t$  = time, seconds

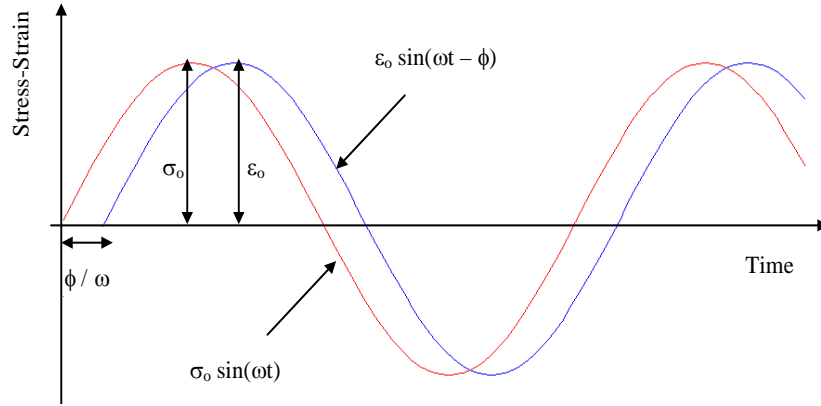


Figure 4 Stress-Strain Cycle, Dynamic Modulus Test.

Mathematically, the dynamic modulus is defined as the absolute value of the complex modulus, or:

$$|E^*| = \frac{\sigma_0}{\epsilon_0}$$

By current practice, dynamic modulus testing of asphalt materials is conducted on unconfined and confined cylindrical specimens having a height to diameter ratio equal to 1.5 and uses a uniaxially applied sinusoidal load (3). Under such conditions, the sinusoidal stress at any given time  $t$ , is given as:

$$\sigma_t = \sigma_0 \sin(\omega t)$$

Where:  $\omega$  = angular frequency in radian per second.

$t$  = time (sec).

The subsequent dynamic strain at any given time is given by:

$$\epsilon_t = \epsilon_0 \sin(\omega t - \phi)$$

The phase angle is simply the angle at which the  $\epsilon_o$  lags  $\sigma_o$ , and is an indicator of the viscous (or elastic) properties of the material being evaluated. Mathematically this is expressed as:

$$\phi = (t_i / t_p) \times (360)$$

Where:

$t_i$  = time lag between a cycle of stress and strain (sec).

$t_p$  = time for a stress cycle (sec).

For a pure elastic material,  $\phi = 0^\circ$ , it is observed that the complex modulus ( $E^*$ ) is equal to the absolute value, or dynamic modulus. For pure viscous materials,  $\phi = 90^\circ$ . The  $E^*$  has a real and imaginary part that defines the elastic and viscous behavior of the linear viscoelastic material:  $E^* = E' + iE''$  and.

$$E' = (\sigma_o / \epsilon_o) \cos \phi$$

$$E'' = (\sigma_o / \epsilon_o) \sin \phi$$

Where:  $\sigma_o$  = peak dynamic stress amplitude (kPa).

$\epsilon_o$  = peak recoverable strain (mm/mm).

$\phi$  = phase lag or angle (degrees).

The  $E'$  value is generally referred to as the storage (elastic) modulus component of the complex modulus, while  $E''$  is referred to as the loss (viscous) modulus. The loss tangent ( $\tan \phi$ ) is the ratio of the energy lost to the energy stored in a cyclic deformation and is equal to:

$$\tan \phi = E'' / E'$$

### 3.2. Master Curve

The modulus of the asphalt mixture at all temperatures and time rate of load is determined from a master curve constructed at a reference temperature (generally taken as 21.1 °C). Master curves are constructed using the principle of time-temperature superposition. The data at various temperatures are shifted with respect to time until the curves merge into single smooth function. The master curve of the modulus, as a function of time, formed in this manner describes the time dependency of the material. The amount of shifting at each temperature required to form the master curve describes the temperature dependency of the material. In general, the master modulus curve can be mathematically modeled by a sigmoidal function described as:

$$\text{Log} |E^*| = \delta + \frac{\alpha}{1 + e^{\beta + \gamma(\log t_r)}}$$

Where,

- $t_r$  = reduced time of loading at reference temperature
- $\delta$  = minimum value of  $E^*$
- $\delta + \alpha$  = maximum value of  $E^*$
- $\beta, \gamma$  = parameters describing the shape of the sigmoidal function

The shift factor can be shown in the following form:

$$a(T) = \frac{t}{t_r}$$

Where,

- $a(T)$  = shift factor as a function of temperature
- $t$  = time of loading at desired temperature
- $t_r$  = time of loading at reference temperature
- $T$  = temperature

While classical viscoelastic fundamentals suggest a linear relationship between  $\log a(T)$  and  $T$  (in degrees Fahrenheit/Celsius); years of testing by various researchers have shown that for precision, a second order polynomial relationship between the logarithm of the shift factor i.e.  $\log a(T_i)$  and the temperature in degrees Fahrenheit ( $T_i$ ) should be used.

The relationship can be expressed as follows:

$$\text{Log } a(T_i) = aT_i^2 + bT_i + c$$

Where,

$a(T_i)$  = shift factor as a function of temperature  $T_i$

$T$  = temperature of interest, °C

$a, b$  and  $c$  = coefficients of the second order polynomial

It should be recognized that if the value of “ $a$ ” approaches zero; the shift factor equation collapses to the classic linear form.

### **3.3. Summary of Test Method**

The AASHTO TP 62-03 was followed for  $E^*$  testing. For each mix, three replicates were used. For each specimen,  $E^*$  tests were conducted at -10, 4.4, 21.1, 37.8 and 54.4 °C and 25, 10, 5, 1, 0.5 and 0.1 Hz loading frequencies. A 60 second rest period was used between each frequency to allow some specimen recovery before applying the new loading at a lower frequency. Table 3 presents a summary of the  $E^*$  test conditions.

Table 3 Test Conditions of the Dynamic Modulus (E\*) Test

Test Temperature (°C)	Freq. (Hz)	Cycles	Rest Period (Sec)	Cycles to Compute E*
-10, 4.4, 21.1, 37.8, 54.4	25	200	-	196 to 200
	10	100	60	196 to 200
	5	50	60	96 to 100
	1	20	60	16 to 20
	0.5	15	60	11 to 15
	0.1	15	60	11 to 15

The E\* tests were conducted using a controlled stress mode with strains smaller than 150 micro-strain. This ensured, to the best possible degree, that the response of the material was linear across the temperatures used. The dynamic stress levels were 69 to 690 kPa for colder temperatures (-10 to 21.1 °C) and 14 to 69 kPa for higher temperatures (37.8 to 54.4 °C). All E\* tests were conducted in a temperature-controlled chamber capable of holding temperatures from -16 to 60 °C.

The axial deformations of the specimens were measured through two spring-loaded Linear Variable Differential Transducers (LVDTs) placed vertically on diametrically opposite sides of the specimen. Parallel brass studs were used to secure the LVDTs in place. Two pairs of studs were glued on the two opposite cylindrical surfaces of a specimen; each stud in a pair, being 100-mm apart and located at approximately the same distance from the top and bottom of the specimen. In order to eliminate any top or bottom surface friction, pairs of rubber membranes, slightly coated with vacuum grease between the membranes, were placed on top and bottom of each specimen during testing. Figure 5 shows the schematic presentation of the instrumentation. Typical test specimens are shown in Figure 6. An instrumented sample used for the E\* test is presented in Figure 7.

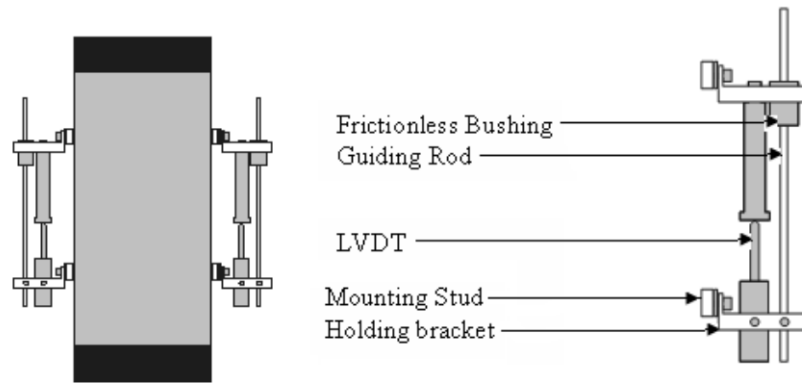


Figure 5 Specimen Instrumentation of E\* Testing.



Figure 6 Malmo E6 External Ring Road Gap Graded Samples.



Figure 7 Typical E\* Test Sample.

### 3.4. Test Results

The quality of the  $E^*$  test data was checked by Black Space diagrams ( $E^*$  versus  $\phi$ ), Cole-Cole Plane plots ( $E^* \sin\phi$  versus  $E^* \cos\phi$ ) and  $E^*$  versus loading frequency ( $\phi$ ) plots.  $E^*$  master curves of all mixtures were constructed for a reference temperature of 21.1 °C using the principle of time-temperature superposition. The time-temperature superposition was done by simultaneously solving for the four coefficients of the sigmoidal function ( $\delta$ ,  $\alpha$ ,  $\beta$ , and  $\gamma$ ) and the three coefficients of the second order polynomial (a, b, and c). The “Solver” function of the Microsoft<sup>TM</sup> Excel was used to conduct the nonlinear optimization for simultaneously solving these 7 parameters. For all mixtures, the set of master curve parameters were obtained for: (i) average  $E^*$  of all replicates, (ii)  $E^*$  of all replicates, and (iii) each replicate. The  $E^*$  of each mix at five test temperatures and six test loading frequencies were also computed using the 7 master curve and shift coefficients. The  $E^*$  data obtained from both laboratory tests are summarized in Tables 4 and 5. The Master curves are shown in Figures 8 and 9.

Table 4 Summary of E\* and Phase Angle values for Unconfined Reference Gap Graded Mix.

Mix	Conf.	Temp.	Freq.	Dynamic Modulus, E* (kPa)					Phase Angle, $\phi$ (degrees)				
	(kPa)	°C	Hz	Rep1	Rep2	Rep3	Avg. E*	%C.V.	Rep1	Rep2	Rep3	Avg. $\phi$	%C.V.
SWR00	0	-10	25	46,397,330	56,451,034	65,483,479	56,110,614	17	3	5	4	4	30
			10	43,249,614	54,161,695	64,202,409	53,871,240	19	7	7	6	13	5
			5	40,996,249	50,880,077	61,854,113	51,243,480	20	9	7	7	13	8
			1	35,383,323	43,773,234	55,185,952	44,780,836	22	10	10	9	15	7
			0.5	32,585,353	40,260,783	51,334,747	41,393,628	23	12	10	9	16	10
			0.1	25,769,299	31,630,046	42,313,294	33,237,547	25	16	14	11	18	13
		4.4	25	23,843,697	30,789,656	41,021,231	31,884,861	27	14	9	11	12	20
			10	20,570,073	24,601,147	36,692,373	27,287,864	31	16	17	15	15	7
			5	18,099,865	19,751,666	31,828,902	23,226,811	32	20	20	17	17	8
			1	13,130,471	14,041,810	22,573,619	16,581,967	31	27	25	23	22	8
			0.5	10,924,073	11,714,499	18,225,774	13,621,448	29	30	28	28	24	4
			0.1	7,251,737	6,937,965	11,127,925	8,439,209	28	37	35	38	30	4
		21.1	25	10,708,229	9,065,421	13,346,315	11,039,988	20	24	28	30	24	13
			10	8,613,749	6,807,060	8,534,806	7,985,205	13	28	32	35	28	12
			5	7,195,778	5,411,073	6,450,319	6,352,390	14	31	35	37	30	11
			1	4,231,929	3,102,748	3,434,508	3,589,728	16	37	39	43	37	8
			0.5	3,347,571	2,422,242	2,616,102	2,795,305	17	38	40	43	39	7
			0.1	2,039,520	1,406,979	1,346,023	1,597,507	24	38	40	42	39	5
		37.8	25	4,792,522	3,276,622	2,497,188	3,522,111	33	33	38	38	36	6
			10	3,232,654	2,079,491	1,688,774	2,333,640	34	37	38	34	35	5
			5	2,389,266	1,528,891	1,295,060	1,737,739	33	36	36	33	34	4
			1	1,344,025	910,339	819,405	1,024,590	27	32	31	31	32	1
			0.5	1,094,206	750,455	703,489	849,384	25	30	28	29	30	3
			0.1	787,429	561,592	557,595	635,539	21	24	24	28	27	9
54.4	25	2,173,423	935,321	830,397	1,313,047	57	37	34	29	32	13		
	10	1,326,038	663,518	658,522	882,693	43	33	28	22	28	20		
	5	1,019,260	551,600	582,577	717,812	36	31	25	22	27	17		
	1	734,467	418,696	523,620	558,928	29	25	20	24	25	10		
	0.5	680,506	389,717	523,640	531,288	27	24	18	27	26	17		
	0.1	623,547	347,748	523,640	498,312	28	24	16	27	32	17		

Table 5 Summary of E\* and Phase Angle values for Unconfined Asphalt Rubber Gap Graded Mix.

Mix	Conf. (kPa)	Temp. °C	Freq. Hz	Dynamic Modulus, E* (kPa)					Phase Angle, $\phi$ (degrees)				
				Rep1	Rep2	Rep3	Avg. E*	%C.V.	Rep1	Rep2	Rep3	Avg. $\phi$	%C.V.
SWG00	0	-10	25	19,205,063	26,890,486	58,395,623	34,830,391	60	7	8	9	8	13
			10	18,572,522	26,525,751	56,250,180	33,782,818	59	9	11	9	13	7
			5	17,889,018	25,604,419	51,795,413	31,762,950	56	10	11	11	13	6
			1	15,637,652	22,280,831	44,341,822	27,420,102	55	11	12	10	15	6
			0.5	14,744,300	21,113,678	41,213,092	25,690,357	54	12	12	13	16	2
			0.1	12,512,920	17,850,046	31,524,123	20,629,030	48	15	14	14	18	2
		4.4	25	11,823,420	17,110,583	27,127,314	18,687,106	42	12	13	10	12	15
			10	10,874,109	15,765,559	23,443,987	16,694,552	38	17	17	14	15	11
			5	10,008,737	14,328,602	21,065,713	15,134,350	37	18	18	15	17	9
			1	7,714,402	10,492,386	15,814,524	11,340,437	36	23	24	20	22	10
			0.5	6,870,015	9,141,366	13,825,967	9,945,782	36	25	26	23	24	7
			0.1	5,050,335	6,154,534	9,896,818	7,033,896	36	31	31	28	30	6
		21.1	25	7,088,856	8,380,918	10,775,181	8,748,318	21	24	22	22	24	5
			10	6,142,542	7,040,891	8,077,139	7,086,857	14	28	29	28	28	3
			5	5,412,073	5,975,664	6,573,230	5,986,989	10	27	32	29	30	8
			1	3,725,297	3,699,315	4,152,986	3,859,199	7	34	38	34	37	6
			0.5	3,125,732	3,017,810	3,333,581	3,159,041	5	36	39	36	39	5
			0.1	2,160,432	1,913,611	1,907,616	1,993,886	7	38	42	37	39	7
		37.8	25	4,061,053	3,170,699	3,121,735	3,451,162	15	31	27	37	36	14
			10	3,115,739	2,701,040	2,185,414	2,667,398	17	30	34	38	35	11
			5	2,521,170	2,159,433	1,651,801	2,110,802	21	29	33	35	34	8
			1	1,705,762	1,334,032	1,007,269	1,349,021	26	33	35	31	32	6
			0.5	1,489,919	1,119,188	831,397	1,146,834	29	32	35	31	30	6
			0.1	1,156,161	793,424	585,575	845,053	34	33	33	27	27	12
		54.4	25	2,346,297	2,402,257	1,676,783	2,141,779	19	33	37	37	32	7
			10	1,628,818	1,640,809	1,130,180	1,466,602	20	32	34	31	28	5
			5	1,224,112	1,211,121	873,366	1,102,866	18	31	32	29	27	5
			1	734,467	736,466	567,588	679,507	14	28	27	24	25	8
			0.5	594,569	621,549	488,645	568,254	12	27	25	22	26	9
			0.1	406,705	468,660	393,714	423,026	9	23	20	17	32	8

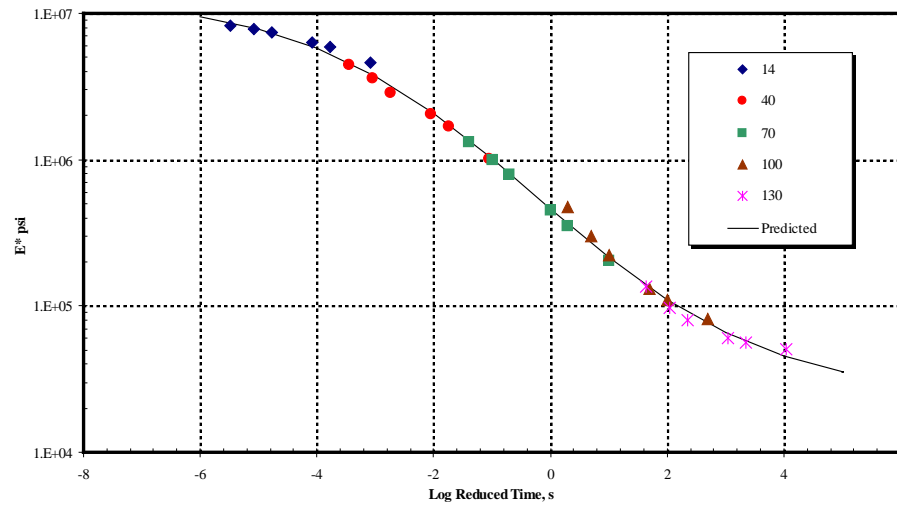
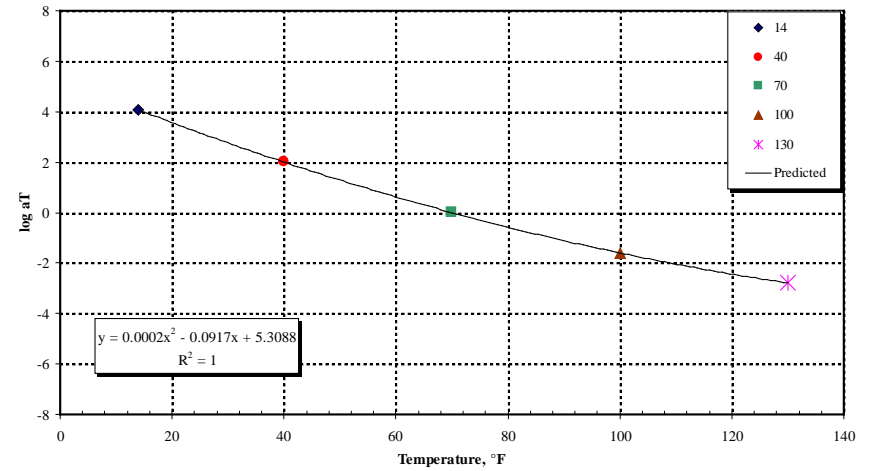
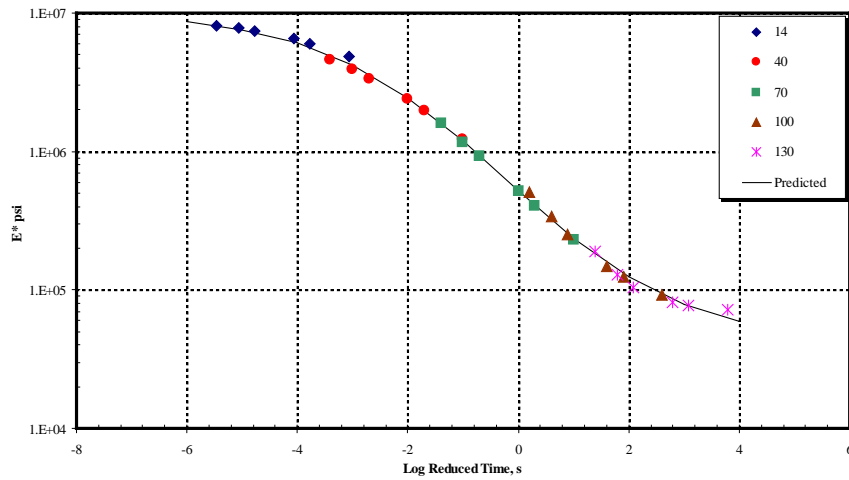


Figure 8 Reference Gap Graded Mix (a) Master Curve based on Average of Three Replicates (b) Shift Factors based on Average of Three Replicates (c) Master Curve of a Typical Replicate.

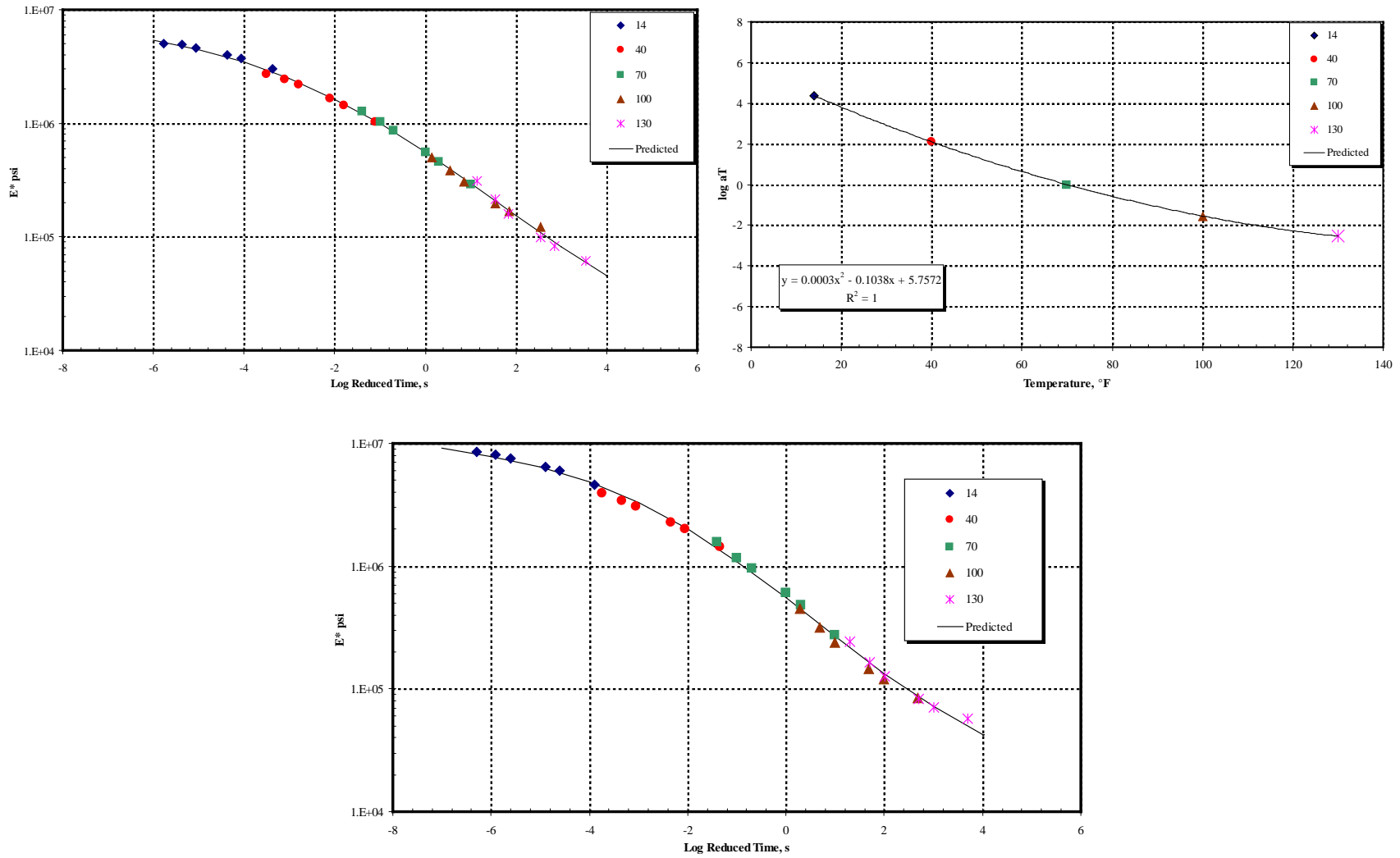


Figure 9 Asphalt Rubber Gap Graded Mix (a) Master Curve based on Average of Three Replicates (b) Shift Factors based on Average of Three Replicates (c) Master Curve of a Typical Replicate.

### 3.5. Mixtures Comparison

Figure 10 shows the average  $E^*$  master curves for both mixtures. The figure can be used for general comparison of the mixtures, but specific temperature-frequency combination values need to be evaluated separately.

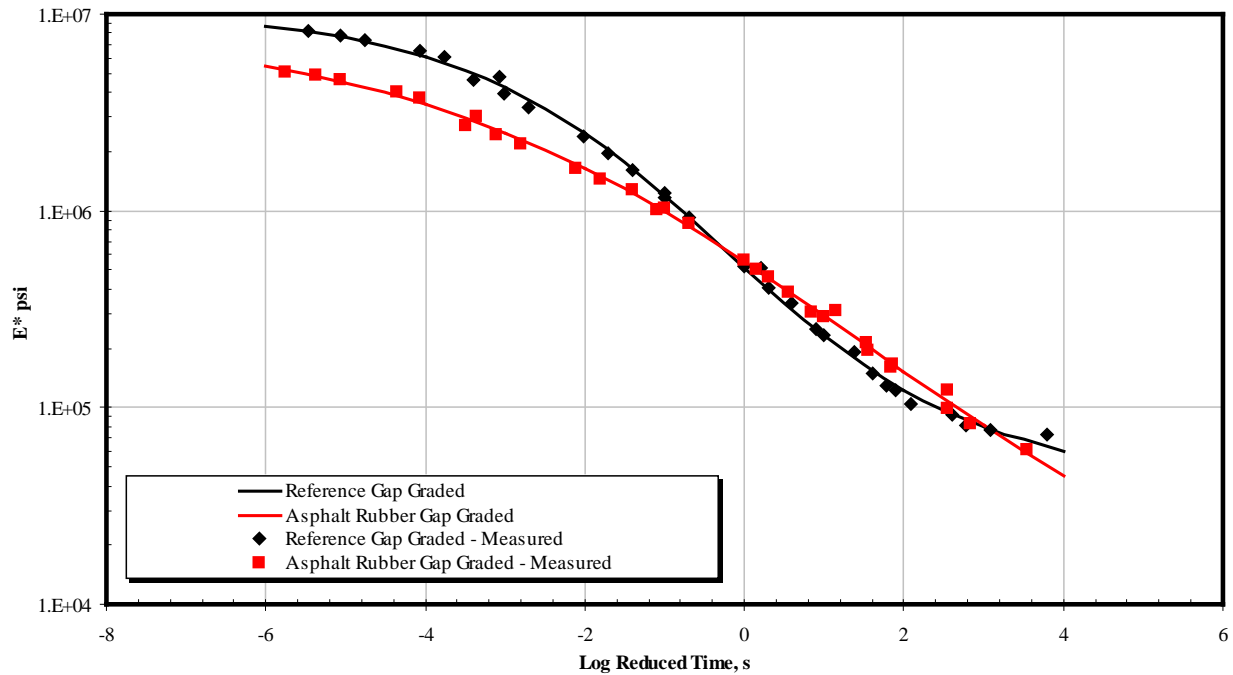


Figure 10 Comparison of  $E^*$  Master Curves.

As it is shown, the reference gap graded mixture shows higher moduli values at lower temperatures (-10 and 4.4 °C) while the trend is reversed with further increase in temperature from 21.1 to 54.4 °C. Lower moduli at cold temperatures are desirable for better resistance of thermal cracking. The increase in moduli values as the temperature increases is also desirable for better resistance to permanent deformation.

The evaluation of modular ratios of asphalt rubber gap graded mixture in contrast to the reference gap graded mix is described below. Modular Ratio (R) of a mix is represented by the following equation.

$$R = \frac{E^*_{MIX}}{E^*_{REFERENCE}}$$

Where:

R = Modular Ratio

$E^*_{MIX}$  = Dynamic Complex Modulus value for a given mixture

$E^*_{REFERENCE}$  = Dynamic Complex Modulus value for the reference mixture

The temperature and frequency conditions used for the comparison were 4.4 °C for lower temperatures, and 37.8 and 54.4 °C for higher temperatures. The frequency selected are 10 Hz, representing vehicle speed typical for an arterial street, and 0.5 Hz, representing much slower vehicle speed such as in the case of parking lots or intersections. For  $E^*$  values at 4.4 °C, the best performance will be that for the mix having lowest  $E^*$  or R. Conversely, at high temperatures, the best mix performance would be for the highest  $E^*$  or R. Table 6 shows ratios of dynamic modulus for the rubber mixture compared to the reference mix.

Table 6 Comparison of Modular Ratios (R).

Conditions	Temperature (°C)	Frequency (Hz)	R = E(AR-Gap)/(Reference Gap)
High Temperatures at Moderate speed	54.4	10	1.66
	37.8	10	1.14
High Temperatures at Low Speed	54.4	0.5	1.07
	37.8	0.5	1.33
Low Temperature at Moderate speed	4.4	10	0.61
	-10	10	0.63
Low Temperature at Low Speed	4.4	0.5	0.73
	-10	0.5	0.62

As can be observed, the modular ratios of asphalt rubber gap graded mix with respect to the reference mix was greater than 1 at higher temperatures and the two test frequencies, a desirable characteristic especially for rutting resistance and for all types of loading conditions. Likewise, at lower temperatures, the modular ratios of asphalt rubber mixtures with respect to the reference mix was lower than 1, also an indication of the rubber-modified mixture's better resistance to low temperature cracking. Figures 11 and 12 show a summary comparison of moduli for selected values of test temperatures (4.4 and 37.8 °C) and loading frequencies (10 and 0.5 Hz).

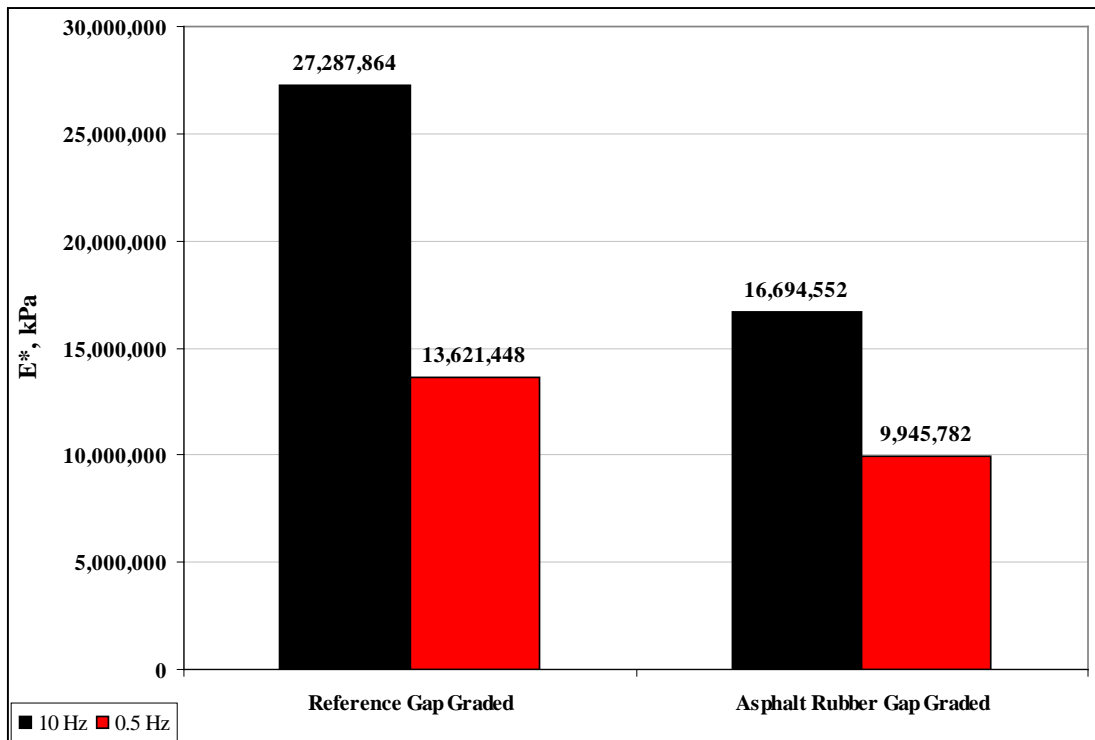


Figure 11 Comparison of Measured Dynamic Modulus  $E^*$  values at 4.4 °C for the Reference and the Asphalt Rubber Gap Graded Mixtures at 10 and 0.5 Hz

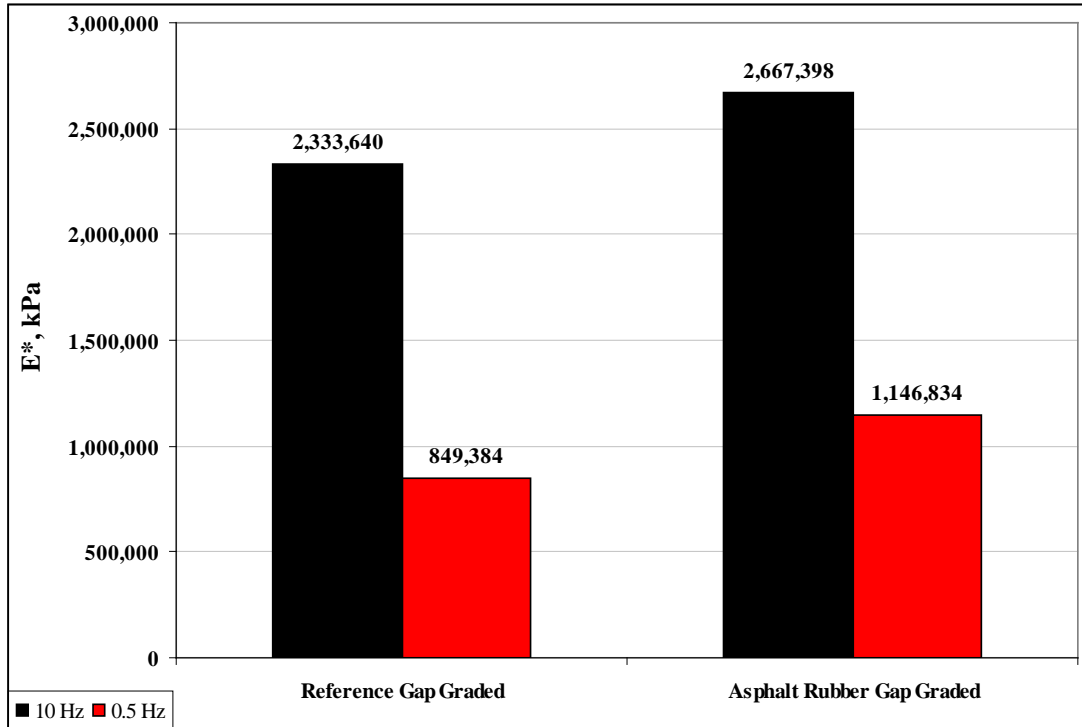


Figure 12 Comparison of Measured Dynamic Modulus  $E^*$  values at 37.8 °C for the Reference and Asphalt Rubber Gap Graded Mixtures at 10 and 0.5 Hz

## 4. REPEATED LOAD PERMANENT DEFORMATION TESTS

### 4.1. Background for the Repeated Load Permanent Deformation Test

An approach to determine the permanent deformation characteristics of paving materials is to employ a repeated dynamic load test for several thousand repetitions and record the cumulative permanent deformation as a function of the number of cycles (repetitions) over the test period. Figure 13 illustrates the typical relationship between the total cumulative plastic strain and number of load cycles. The cumulative permanent strain curve is generally defined by three zones: primary, secondary, and tertiary. In the primary zone, permanent deformations accumulate rapidly. The incremental permanent deformations decrease reaching a constant value in the secondary zone. Finally, the incremental permanent deformations again increase and permanent deformations accumulate rapidly in the tertiary zone. The starting point, or cycle number, at which tertiary flow occurs, is referred to as the “Flow Number” (3).

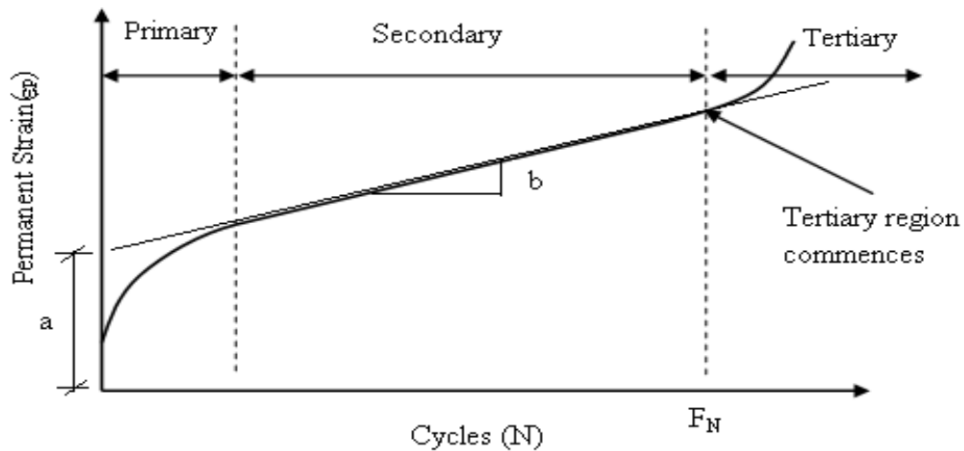


Figure 13 Typical Relationship between Total Cumulative Plastic Strain and Number of Load Cycles

#### 4.2. Test Conditions for the Repeated Load Tests

Because of the limited mixture availability for testing in this study, the samples that were used for E\* Dynamic Modulus test evaluation were used to run the repeated load permanent deformation tests. Repeated load tests were conducted using three replicate test specimens for both reference gap graded and asphalt rubber gap graded mixtures. All tests were carried out on cylindrical specimens, 100 mm in diameter and 150 mm in height. Figure 14 shows a photograph of an actual specimen set-up for unconfined test. Thin and fully lubricated membranes at the test specimen ends were used to warrant frictionless surface conditions. All tests were conducted within an environmentally controlled chamber throughout the testing sequence (i.e., temperature was held constant within the chamber to  $\pm 0.5$  °C throughout the entire test). The tests were conducted unconfined at 30 °C and at a stress level of 1,034 kPa (150 psi).

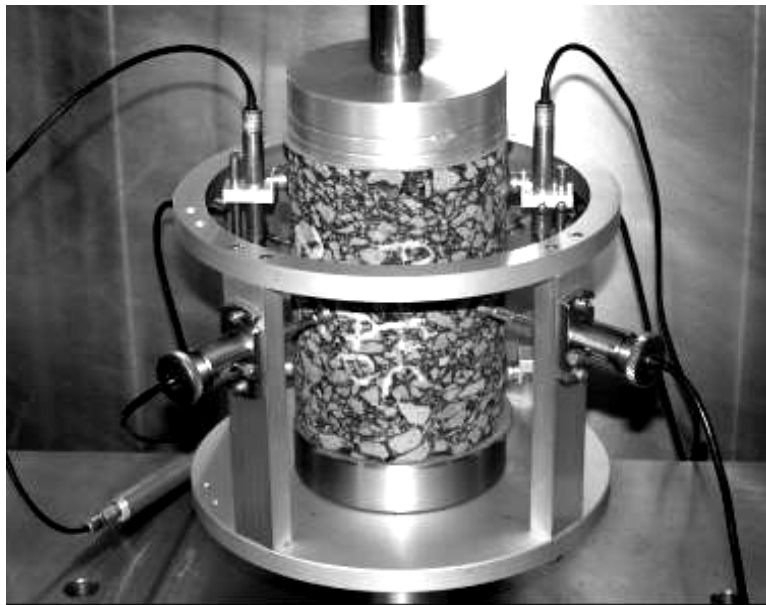


Figure 14 Vertical and Radial LVDTs Set Up for an Unconfined Test

### 4.3. Repeated Load / Flow Number Test Results and Analysis

#### 4.3.1 Results and Analysis

The results for the repeated load unconfined tests are summarized in this section. Table 7 contains the test results with the final average values used for the analysis and comparison of the two mixtures. Table 7 includes the flow number, percent of axial strain at failure (flow), Resilient Modulus at failure, and the permanent deformation parameters (a–intercept and b–slope).

Table 7 Master Summary of Repeated Load Test Results, Swedish Malmo E6 Mixtures.

Mix	Target VA (%)	Temp (°C)	$\sigma_3$ (kPa)	$\sigma_d$ (kPa)	Axial Flow Number (Cycles)	Axial Strain (%)	Resilient Modulus @ Failure (MPa)	Intercept a (1/MPa)	Slope b
Reference Gap graded	2	30	0	1034	1,396	1.61	256	0.0184	0.6144
	2	30	0	1034	906	1.89	343	0.0257	0.6301
	2	30	0	1034	431	2.31	331	0.0325	0.7000
	Average				911	1.94	310	0.0255	0.6482
AR Gap graded	2	30	0	1034	2,566	1.13	294	0.0098	0.6044
	2	30	0	1034	4,836	1.09	312	0.0042	0.6549
	2	30	0	1034	7,476	1.54	288	0.0029	0.7014
	Average				4,959	1.26	298	0.0056	0.6536

Figure 15 presents the Flow Number results for the unconfined tests performed on the two mixtures. The results show that AR-Gap graded mixture had higher flow number values with an average FN of 4,959 cycles than the Reference-Gap graded mixture whose average FN was 911 cycles. Since the average FN of the AR-Gap graded mixture were about 5.5 times higher than the Reference-Gap graded mixture, the AR-Gap graded mixture would be less susceptible to permanent deformation.

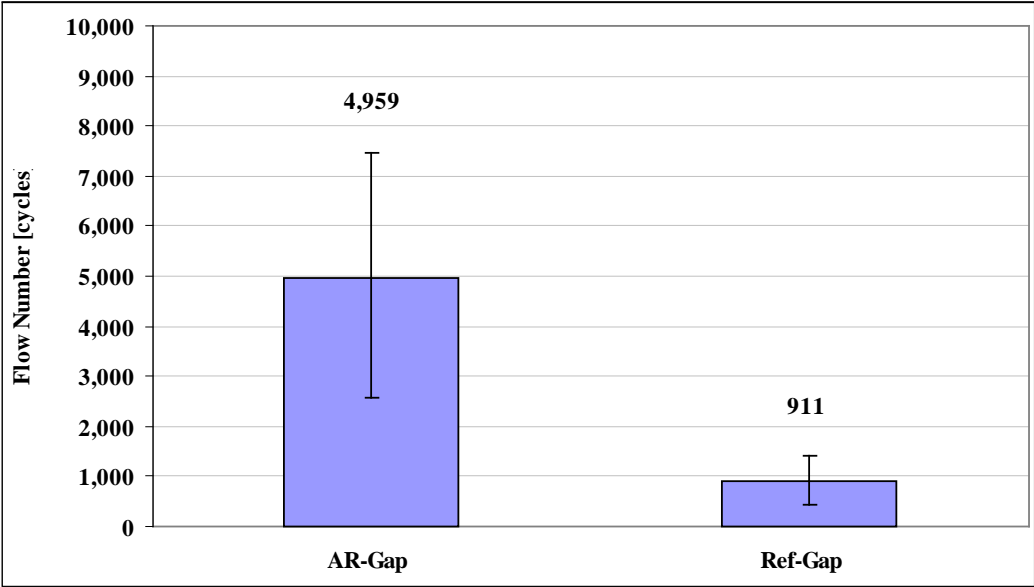


Figure 15 Repeated Load Permanent Deformation Flow Number Test Results, Swedish Malmo E6 Gap Graded Mixtures

## **5.FATIGUE CRACKING TESTS**

### **5.1. Background of the Flexural Beam Fatigue Test**

Load associated fatigue cracking is one of the major distress types occurring in flexible pavement systems. The action of repeated loading caused by traffic induced tensile and shear stresses in the bound layers, which will eventually lead to a loss in the structural integrity of a stabilized layer material. Fatigue initiated cracks at points where critical tensile strains and stresses occur. Additionally, the critical strain is also a function of the stiffness of the mix. Since the stiffness of an asphalt mix in a pavement layered system varies with depth; these changes will eventually effect the location of the critical strain that varies with depth; these changes will eventually effect the location of the critical strain that causes fatigue damage. Once the damage initiates at the critical location, the action of traffic eventually causes these cracks to propagate through the entire bound layer.

Over the last 3 to 4 decades of pavement technology, it has been common to assume that fatigue cracking normally initiates at the bottom of the asphalt layer and propagates to the surface (bottom-up cracking). This is due to the bending action of the pavement layer that results in flexural stresses to develop at the bottom of the bound layer. However, numerous recent worldwide studies have also clearly demonstrated that fatigue cracking may also be initiated from the top and propagates down (top-down cracking). This type of fatigue is not as well defined from a mechanistic viewpoint as the more classical “bottom-up” fatigue. In general, it is hypothesized that critical tensile and/or shear stresses develop at the surface and cause extremely large contact pressures at the tire edges-pavement interface this, coupled with highly aged (stiff) thin surface layer that have become oxidized is felt to be responsible for the surface cracking that

develops. In order to characterize fatigue in asphalt layers, numerous model forms can be found in the existing literature. The most common model form used to predict the number of load repetitions to fatigue cracking is a function of the tensile strain and mix stiffness (modulus). The basic structure for almost every fatigue model developed and presented in the literature for fatigue characterization is of the following form (4):

$$N_f = K_1 \left( \frac{1}{\varepsilon_t} \right)^{k_2} \left( \frac{1}{E} \right)^{k_3} = K_1 (\varepsilon_t)^{-k_2} (E)^{-k_3} \quad (5.1)$$

Where:

$N_f$  = number of repetitions to fatigue cracking

$\varepsilon_t$  = tensile strain at the critical location

$E$  = stiffness of the material

$K_1, K_2, K_3$  = laboratory calibration parameters

In the laboratory, two types of controlled loading are generally applied for fatigue characterization: constant stress and constant strain. In constant stress testing, the applied stress during the fatigue testing remains constant. As the repetitive load causes damage in the test specimen the strain increases resulting in a lower stiffness with time. In case of constant strain test, the strain remains constant with the number of repetitions. Because of the damage due to repetitive loading, the stress must be reduced resulting in a reduced stiffness as a function of repetitions. The constant stress type of loading is considered applicable to thicker pavement layers usually more than 200 mm. For AC thicknesses between these extremes, fatigue behavior is governed by a mixed mode of loading, mathematically expressed as some model yielding intermediate fatigue prediction to the constant strain and stress conditions.

## 5.2. Testing Equipment

Flexural fatigue tests are performed according to the AASHTO T321 (5), and SHRP M-009 (6). The flexural fatigue test has been used by various researchers to evaluate the fatigue performance of pavements (7, 8, 9). Figure 16 shows the flexural fatigue apparatus. The device is typically placed inside an environmental chamber to control the temperature during the test.

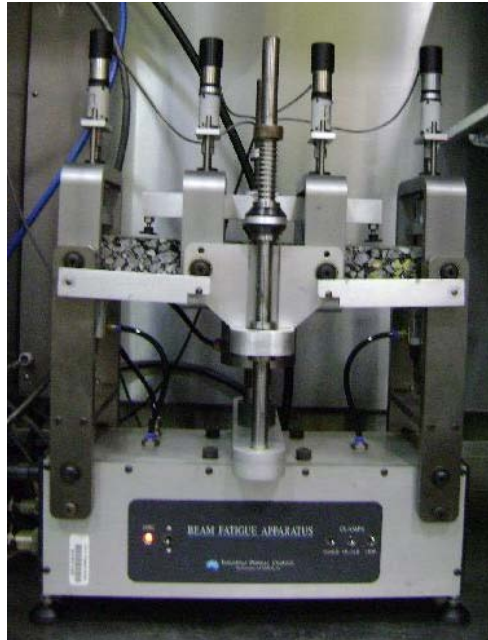


Figure 16 Flexural Fatigue Apparatus

The cradle mechanism allows for free translation and rotation of the clamps and provides loading at the third points as shown in Figure 17. Pneumatic actuators at the ends of the beam center it laterally and clamp it. Servomotor driven clamps secure the beam at four points with a pre-determined clamping force. Haversine or sinusoidal loading may be applied to the beam via the built-in digital servo-controlled pneumatic actuator. The innovative “floating” on-specimen transducer measures and controls the true beam deflection irrespective of loading frame compliance. The test is run under either a controlled strain or a controlled stress loading.

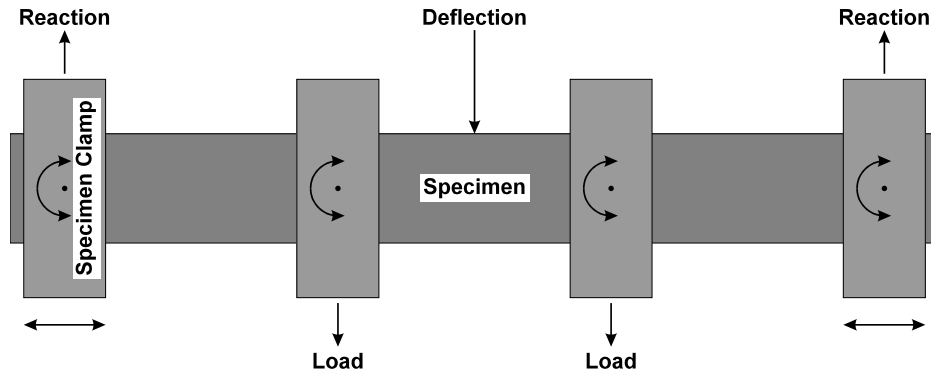


Figure 17 Loading Characteristics of the Flexural Fatigue Apparatus

In the constant stress mode, the stress remains constant but the strain increases with the number of load repetitions. In the constant strain test, the strain is kept constant and the stress decreases with the number of load repetitions. In either case, the initial deflection level is adjusted so that the specimen will undergo a minimum of 10,000 load cycles before its stiffness is reduced to 50 percent or less of the initial stiffness. In this study, all tests were conducted in the control strain type of loading.

### 5.3. Test Procedure and Calculations

The test utilized in this study applied repeated third-point loading cycles as was shown in above figure. The sinusoidal load was applied at a frequency of 10 Hz. The maximum tensile stress and maximum tensile strain were calculated as:

$$\sigma_t = 0.357 P / b h^2 \quad (5.2)$$

$$\varepsilon_t = 12 \delta h / (3 L^2 - 4 a^2) \quad (5.3)$$

where,

$\sigma_t$  = Maximum Tensile stress, Pa

$\varepsilon_t$  = Maximum Tensile strain, m/m

P = Applied load, N

$b$  = Average specimen width, m  
 $h$  = Average specimen height, m  
 $\delta$  = Maximum deflection at the center of the beam, m  
 $a$  = Space between inside clamps, 0.357/3 m (0.119 m)  
 $L$  = Length of beam between outside clamps, 0.357 m

The flexural stiffness was calculated as follow.

$$E = \sigma_t / \varepsilon_t \quad (5.4)$$

where,

$E$  = Flexural stiffness, Pa

The phase angle ( $\phi$ ) in degrees was determined as follow.

$$\phi = 360 f s \quad (5.5)$$

where,

$f$  = Load frequency, Hz

$s$  = Time lag between  $P_{\max}$  and  $\delta_{\max}$ , seconds

The dissipated energy per cycle and the cumulative dissipated energy were computed using Equations 4.6 and 4.7, respectively.

$$w = \pi \sigma_t \varepsilon_t \sin \phi \quad (5.6)$$

$$\text{Cumulative Dissipated Energy} = \sum_{i=1}^{i=N} w_i \quad (5.7)$$

where,

$w$  = Dissipated energy per cycle, J/m<sup>3</sup>

$w_i$  =  $w$  for the  $i^{\text{th}}$  load cycle

During the test the flexural stiffness of the beam specimen was reduced after each load cycle. The stiffness of the beam was plotted against the load cycles; the data was best fitted to an exponential function as follow.

$$E = E_i e^{bN} \quad (5.8)$$

where,

$E$  = Flexural stiffness after  $n$  load cycles, Pa

$E_i$  = Initial flexural stiffness, Pa

$e$  = Natural logarithm to the base  $e$

$b$  = Constant

$N$  = Number of load cycles

Once Equation 4.8 was formulated, the initial stiffness  $S_i$  can be obtained. Failure was defined as the point at which the specimen stiffness is reduced to 50 percent of the initial stiffness. The number of load cycles at which failure occurred was computed by solving Equation 4.8 for  $N$ , or simply:

$$N_{f,50} = [\ln (E_{f,50} / E_i)] / b \quad (5.9)$$

where,

$N_{f,50}$  = Number of load cycles to failure

$E_{f,50}$  = Stiffness at failure, Pa

## **5.4. Materials and Specimen Preparation**

### **5.4.1. Materials**

All beam specimens were prepared using the reheated reference and asphalt rubber mixtures that were obtained during construction.

#### **5.4.2. Mold Assembly**

The AASHTO TP8-94, and SHRP M-009, flexural fatigue testing protocol, require preparation of oversize beams that later have to be sawed to the required dimensions. The final required dimensions are  $380 \pm 6$  mm in length,  $50 \pm 6$  mm in height, and  $63 \pm 6$  mm in width. The procedure does not specify a specific method for preparation. Several methods have been used to prepare beam molds in the laboratory including full scale rolling wheel compaction, miniature rolling wheel compaction, and vibratory loading.

In this study beams were prepared using vibratory loading applied by a servo-hydraulic loading machine. A beam mold was manufactured at ASU with structural steel that is not hardened. The mold consists of a cradle and two side plates as shown in Figure 18. The inside dimensions of the mold are 12 mm larger than the required dimensions of the beam after sawing in each direction to allow for a 6 mm sawing from each face. A top loading platen was originally connected to the loading shaft assembly in the middle as shown in Figure 19. Note that the top platen is made of a series of steel plates welded at the two ends to distribute the load more evenly during compaction. The loading shaft was connected to the upper steel plate rather than extending it to the bottom plate so that an arch effect is introduced that would assist in distributing the load more uniformly. In addition, it was found that if the bottom surface of the bottom plate is machined to be slightly concave upward, it would counter balance any bending that might occur during compaction and produce more uniform air void distribution.



Figure 18 Manufactured Mold for Beam Compaction



Figure 19 Top Loading Platen

### 5.4.3. Specimen Preparation

Both mixtures were heated at 146 °C. The mold was heated separately for one hour at the same temperature as the mix. The mixture was placed in the mold in one load. The mold was then placed on the bottom plate of the loading machine and the top platen was lowered to contact the mixture. A small load of 1.4 kPa was then applied to seat the specimen. A stress-controlled sinusoidal load was then applied with a frequency of 2 Hz and a peak-to-peak stress of 2.8 MPa for the compaction process. Since the height of the specimen after compaction was fixed, the

weight of the mixture required to reach a specified air void value was pre-calculated. Knowing the maximum theoretical specific gravity and the target air voids, the weight of the mixture was determined. During compaction the loading machine was programmed to stop when the required specimen height was reached.

After compaction, specimens were left to cool to ambient temperature. The specimens were brought to the required dimensions for fatigue testing by sawing 6 mm from each side (Figure 20). The specimens were cut by using water cooled saw machine to the standard dimension of 63.5 mm wide, 51 mm high, and 381 mm long. Finally, the air void content was measured by using the saturated surface-dry procedure (AASHTO T166, Method A). Figure 21 shows typical reference and asphalt rubber gap graded beams.



Figure 20 Beam specimen sawing.

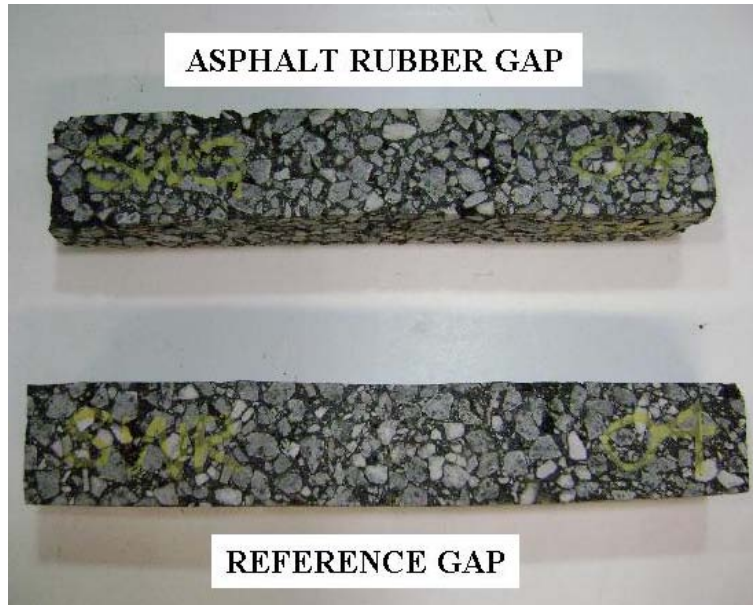


Figure 21 Typical Reference and Asphalt Rubber Beams. (Photos taken after test)

### 5.5. Testing Factorial

The following conditions were used:

- Air voids: 2.0% for the reference gap and AR gap specimens.
- Load condition: Constant strain level, 4 levels of the range (175-425  $\mu$  strain).
- Load frequency: 10 Hz.
- Test temperature: 21.1 °C.

Initial flexural stiffness was measured at the 50<sup>th</sup> load cycle. Fatigue life or failure under control strain was defined as the number of cycles corresponding to a 50% reduction in the initial stiffness. The loading was also extended to reach a final stiffness of 30%. The control and acquisition software load and deformation data were reported at predefined cycles spaced at logarithmic intervals.

## 5.6. Test Results and Analysis

Tabular summaries of the fatigue test results and regression coefficients are presented in Tables 8 and 9. Table 10 shows summary of regression coefficients for the fatigue relationships at 50% of initial stiffness. The relationships obtained were excellent in terms of models accuracy as indicated by the coefficient of determination ( $R^2$ ).

Fatigue relationships (flexural strain versus the number of loading cycles) for each mixture are shown in Figures 22 and 23. The figures show a very interesting trend and relationship between both mixtures at 21.1 °C, for 50 and 30% of the initial stiffness values. At high strain values, it is noticed from both figures that the fatigue life is higher for the Reference mix when compared to the AR mix. However, at lower strains, the AR mixture has higher fatigue life. Since the pavement sections are part of a highway, the expected fatigue life for the AR gap graded mixture is higher than the reference mix as the strain level conditions are anticipated to be lower (~80 km/h vehicle speed). If the same two mixtures are used on roads with lower design speeds (such as parking lots and intersections), it is anticipated that the reference mixture will provide higher fatigue life than the AR gap graded mixture.

Table 8 Control Strain Beam Fatigue Test Results for the Reference Gap Graded Mixture.

Beam #	Temp [°C]	Air Void %	Width (mm)	Ht. (mm)	Strain Level (μ)	Initial Stiffness (10 <sup>3</sup> psi)		50% of Initial Stiffness				30% of Initial Stiffness			
						50 cycles	100 cycles	Stiffness (KPa)	Cycles	Phase Angle	Cum. Energy (KPa)	Stiffness (KPa)	Cycles	Phase Angle	Cum. Energy (KPa)
SWR04	21	2.105	65.3	54.4	350	830.6	834.9	2857172	229,080	35.5	46865	1716214	446,680	30.4	78676
SWR01	21	2.021	66.0	53.1	700	678.8	645.1	2339907	9,690	46.1	7052	1401144	39,400	42.7	21282
SWR02	21	2.199	65.9	50.0	850	563.2	528.8	1941564	5,600	46.1	5324	1164938	20,150	42.2	14312

Table 9 Control Strain Beam Fatigue Test Results for the Asphalt Rubber Gap Graded Mixture.

Beam #	Temp [°C]	Air Void %	Width (mm)	Ht. (mm)	Strain Level (μ)	Initial Stiffness (10 <sup>3</sup> psi)		50% of Initial Stiffness				30% of Initial Stiffness			
						50 cycles	100 cycles	Stiffness (KPa)	Cycles	Phase Angle	Cum. Energy (KPa)	Stiffness (KPa)	Cycles	Phase Angle	Cum. Energy (KPa)
SWG04	21	2.057	66.3	50.6	400	423.6	420.2	1458561	420,080	7.9	28270	873374	602,550	3.1	34926
SWG01	21	2.016	66.3	50.7	600	419.4	407.1	1445693	29,580	29.7	8410	867429	99,740	31.4	23178
SWG02	21	2.007	64.6	51.0	750	434.5	412.7	1497955	4,410	29.5	2125	898801	11,040	31.5	4373

Table 10 Summary of Regression Coefficients for the Fatigue Relationships at 50% of Initial Stiffness, Swedish Mixtures, 21.1 °C

Mix Type	k1	k2	R <sup>2</sup>
Reference Gap Graded Mixture	0.0061	-0.2322	0.9948
AR Gap Graded Mixture	0.0024	-0.1389	0.9949

\*  $N_f = K_1 * (1/\epsilon_t)^{K2}$

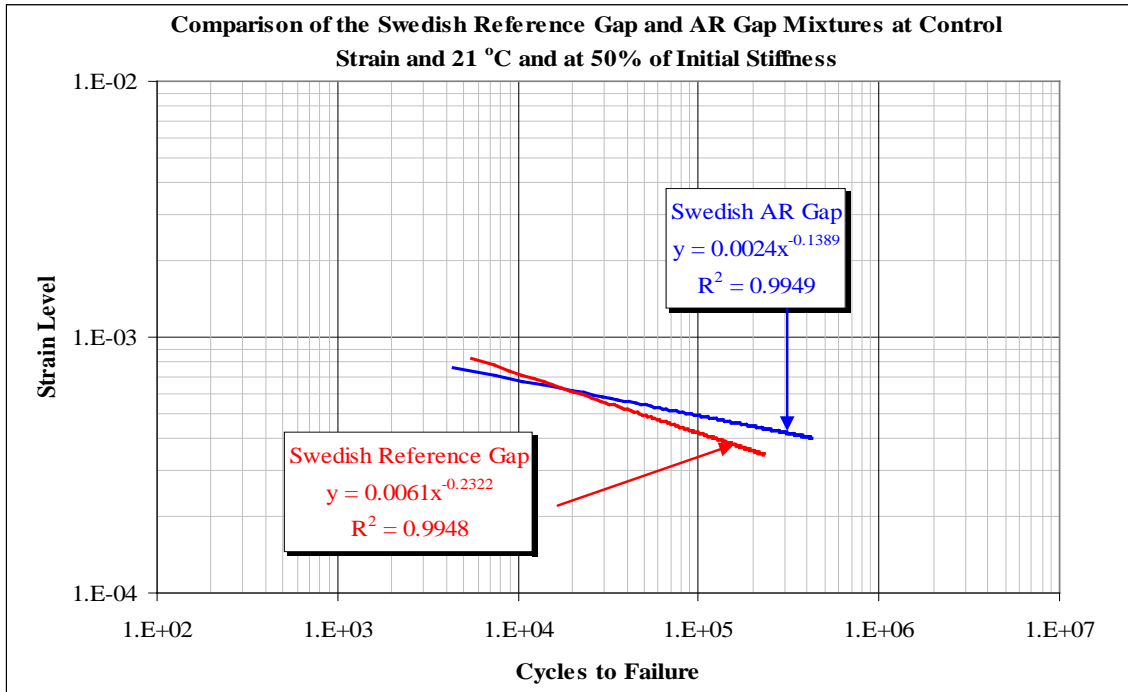


Figure 22 Comparison of Fatigue Relationships at 50% of Initial Stiffness.

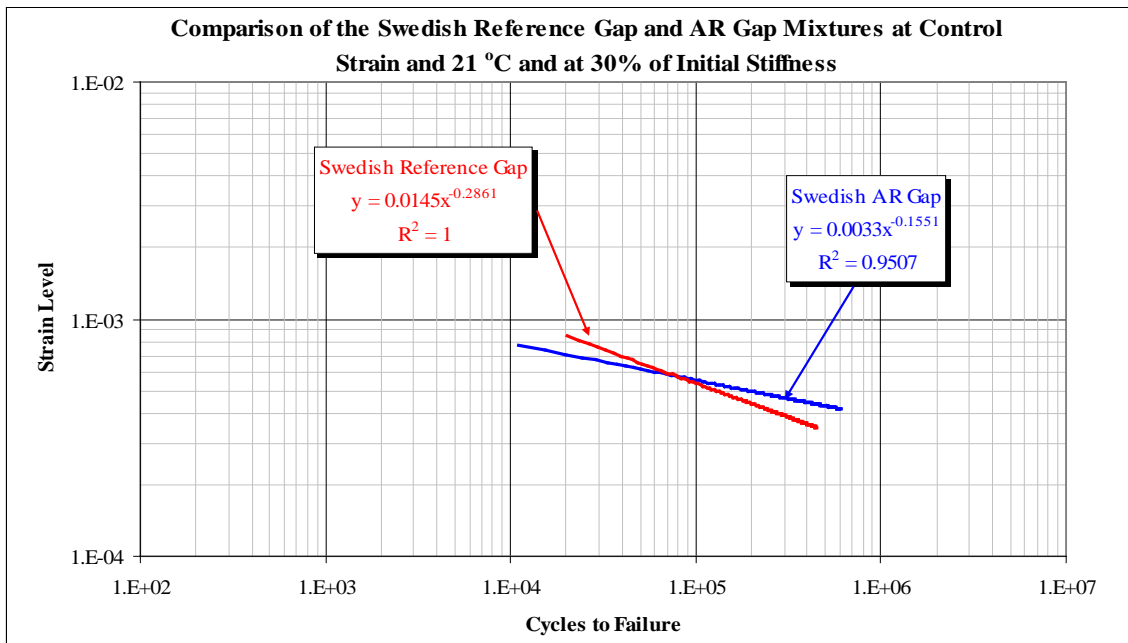


Figure 23 Comparison of Fatigue Relationships at 30% of Initial Stiffness.

## **6. CRACK PROPAGATION TEST – C\* LINE INTEGRAL**

### **6.1. Background**

Fracture mechanics provides the underlying principles which govern the initiation and propagation of cracks in materials. Sharp internal or surface notches which exist in various materials intensify local stress distribution. If the energy stored at the vicinity of the notch is equal to the energy required for the formation of new surfaces, then crack growth can take place. Material at the vicinity of the crack relaxes, the strain energy is consumed as surface energy, and the crack grows by an infinitesimal amount. If the rate of release of strain energy is equal to the fracture toughness, then the crack growth takes place under steady state conditions and the failure is unavoidable (10, 11).

The concept of fracture mechanics was first applied to asphalt concrete by Majidzadeh (12). Abdulshafi (13) has applied the energy (C\*-Line Integral) approach to predicting the pavement fatigue life using the crack initiation, crack propagation, and failure. He concluded that two different tests are required to evaluate first the fatigue life to crack initiation (conventional fatigue testing) and second, the crack propagation phase using notched specimen testing under repeated loading. Abdulshafi and Majidzadeh (11) used notched disk specimens to apply J-integral concept to the fracture and fatigue of asphalt pavements. Various situations such as the effect of load magnitude on fatigue cracking, the length of rest period, load sequence, support conditions, and temperature were included in the testing protocol. Several research studies have also been conducted to apply fracture mechanics principles on asphaltic materials.

## 6.2. C\* Parameters

The relation between the J-integral and the C\* parameters is a method for measuring it experimentally. J is an energy rate and C\* is an energy rate or power integral. An energy rate interpretation of J has been discussed by Rice and Begley and Landes (14, 15). J can be interpreted as the energy difference between the two identically loaded bodies having incrementally differing crack lengths.

$$J = - \frac{dU}{da}$$

Where

U = Potential Energy

a = Crack Length

C\* can be calculated in a similar manner using a power rate interpretation. Using this approach C\* is the power difference between two identically loaded buddies having incrementally differing crack lengths.

$$C^* = - \frac{\partial U^*}{\partial a}$$

Where

U\* is the power or energy rate defined for a load p and displacement u by

$$U^* = \int_0^u p du$$

Abdulshafi and Kaloush demonstrated the use of C\* line integral test in a research study for the US Air Force (16). In their study, several modified asphalt mixtures were evaluated for their potential resistance to crack propagation. The results are shown in Figure 24. The AC-20 line represents the control mix used in the Air Force study. Mixtures with higher slopes

(above the AC-20 line) are ones that have higher resistance to crack propagation. Higher the slope, better the resistance.

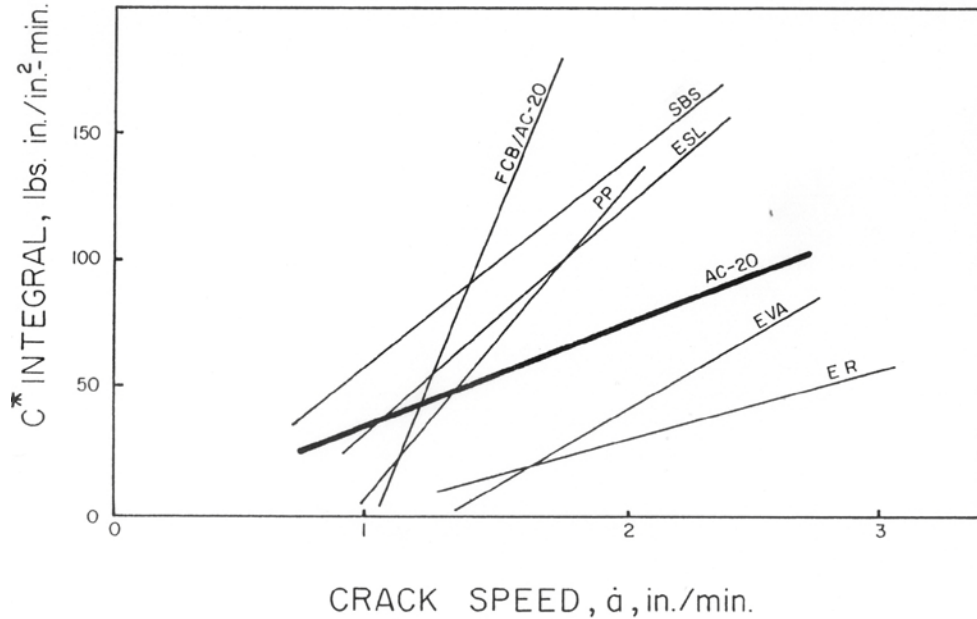


Figure 24 C\* Integral Test Results for Several Modified Asphalt Mixtures (16).

### 6.3. Test Specimen and Test Conditions

The test samples were prepared according to the Test Protocol UMD 9808, "Method for Preparation of Triaxial Specimens" (17). The specimens were reheated and compacted with a Servopac gyratory compactor into a 150-mm diameter gyratory mold to approximately 160-mm in height. Approximately 5-mm was sawed from each end of the compacted specimen, and 3 test specimens approximately 38-mm thick were cut from each compacted specimen.

A right-angle wedge was cut into the specimens to accommodate the loading device. An IPC Universal Testing Machine (UTM 25) electro-pneumatic system was used to load the specimens. The machine is equipped to apply 25 kN maximum vertical load. The load was

measured through the load cell. The test setup is shown in Figure 25. All tests were conducted at room temperature  $\sim 21.1^\circ \text{C}$ . Figure 26 shows typical samples.

The experimental testing involves collecting the data as load and crack length versus time for a constant displacement rate. This information is used to determine load as a function of displacement rate for various crack lengths, and crack growth rate versus crack length. The power of energy rate input,  $U^*$ , is measured as the area under the load displacement rate curve. The energy rate,  $U^*$ , is then plotted versus crack length for different displacement rates and the slopes of these curves constitute the  $C^*$ -integral. The  $C^*$ -integral is plotted as a function of the displacement rate. Finally, the crack growth rate is plotted as a function of  $C^*$  integral. The steps of this process are described in detail in the next section.

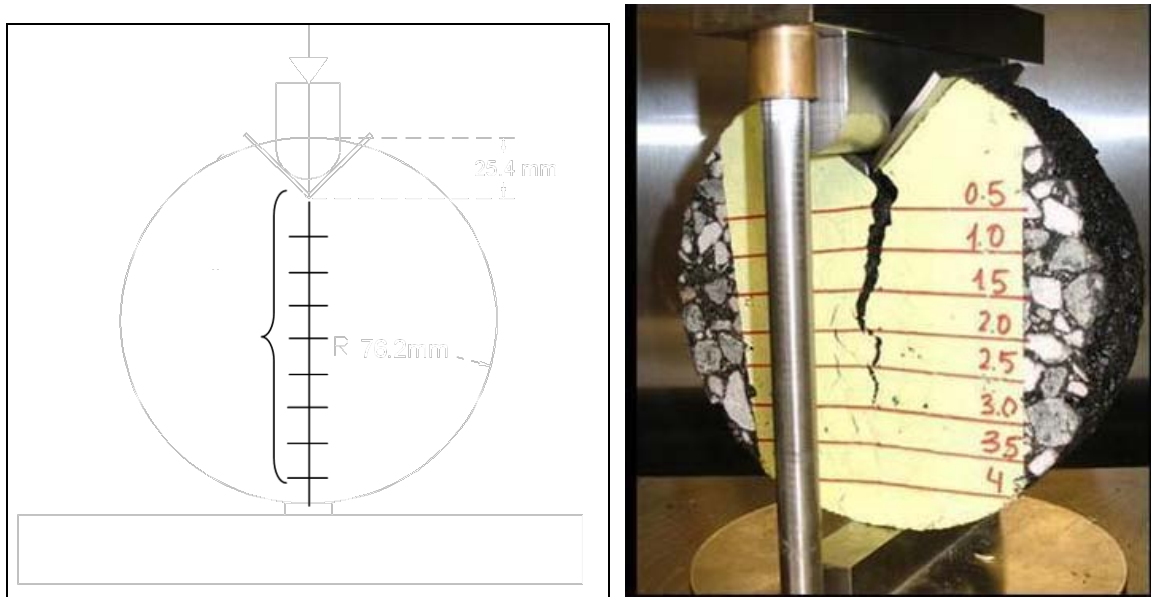


Figure 25 Typical  $C^*$  Test Setup



Figure 26 Typical C\* Test Samples

#### 6.4. Method for C\* Determination

For multiple specimens tested at different displacement rates, the data are collected as load and crack length versus time for a constant displacement rate. The tested samples and displacement rates are shown in Table 11 for the reference and asphalt rubber gap graded mixtures.

Table 11 Displacement Rates Used for Both Mixtures.

Displacement Rate, $\Delta^*$ (mm/min)	Reference Gap	Rubber Gap
0.38	SWR04T	SWG04B
0.51	SWR04M	SWG04M
0.64	SWR04B	SWG04T
0.76	SWR05T	SWG05M
0.89	SWR06T	SWG05T

The calculations are achieved through six main steps as follows:

1. The load value is adjusted taking into consideration the sample thickness. This is done by dividing the load value by the sample thickness; then the load and crack length versus time are plotted for each displacement rate.
2. The load and the displacement rates are plotted for each crack length.
3. The energy rate input  $U^*$  is measured as the area under the curve in step 2. Since the value of each displacement rate is required, an area for each rate was assigned as shown in Figure 27. The areas were calculated by integrating the equation of the trend line that represents this relation. For each area, its boundary was used in the integration process. To get five area values, the trend line was extended for half spacing from the beginning and the end so that each displacement rate represents the center of its area. After that, the  $U^*$  values were obtained and plotted versus crack length for each displacement rate. The slope of these curves are  $C^*$  value for each displacement rate. Figures 28 and 29 show the Crack Length versus Energy Rate for the two mixes.
4. The  $C^*$  values versus the Displacement rate are plotted for both mixtures.
5. The crack growth rates were calculated for each displacement rate as the total crack length divided by the time. These values also were corrected according to the sample thickness. The crack growth rate versus the displacement rate values were plotted for both the mixtures.

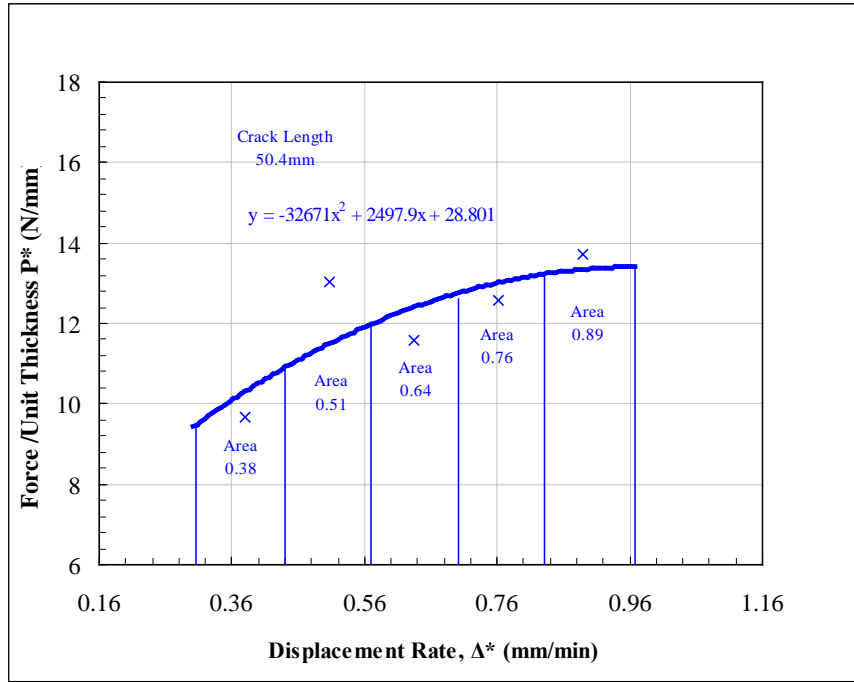


Figure 27 Method of Area Calculations.

- The crack growth rate versus the  $C^*$  values are plotted for the two mixes to compare the performance of each mix through the slope of this relationship where the higher the slope the higher the resistance of the mix to crack propagation. Tables 12 and 13 present summary of test results for all the two mixes.

Table 12 Summary of Test Results for the Reference Gap Mix.

Crack Length, a (mm)	Time T, (Min)	Force, P (N)	Force per Unit Thickness P* (N/mm)	Crack Growth Rate, a* (mm/min)
<b>Sample ID:</b>		<b>Thickness, b (mm):</b>	<b>Displacement Rate, <math>\Delta^*</math> (mm/min) :</b>	
<b>SWR04T</b>		<b>43.18</b>	<b>0.381</b>	
12.7	9.7	460.0	10.7	<b>4.882</b>
25.4	16.3	350.0	8.1	
38.1	18.3	210.0	4.9	
50.8	19.3	170.0	3.9	
63.5	23.4	130.0	3.0	
76.2	27.2	70.0	1.6	
88.9	41.8	50.0	1.2	
<b>Sample ID:</b>		<b>Thickness, b (mm):</b>	<b>Displacement Rate, <math>\Delta^*</math> (mm/min) :</b>	
<b>SWR04M</b>		<b>47.75</b>	<b>0.508</b>	
12.7	9.7	1029.2	21.6	<b>6.187</b>
25.4	7.9	979.2	20.5	
38.1	10.0	899.3	18.8	
50.8	12.5	529.6	11.1	
63.5	14.0	409.7	8.6	
76.2	18.8	229.8	4.8	
88.9	33.0	99.9	2.1	
<b>Sample ID:</b>		<b>Thickness, b (mm):</b>	<b>Displacement Rate, <math>\Delta^*</math> (mm/min) :</b>	
<b>SWR04B</b>		<b>46.74</b>	<b>0.635</b>	
12.7	6.5	979.9	21.0	<b>7.021</b>
25.4	7.6	959.9	20.5	
38.1	10.2	899.9	19.3	
50.8	11.8	709.9	15.2	
63.5	14.7	619.9	13.3	
76.2	17.8	460.0	9.8	
88.9	26.3	300.0	6.4	
<b>Sample ID:</b>		<b>Thickness, b (mm):</b>	<b>Displacement Rate, <math>\Delta^*</math> (mm/min) :</b>	
<b>SWR05T</b>		<b>48.26</b>	<b>0.762</b>	
12.7	7.1	1069.9	22.2	<b>5.961</b>
25.4	9.6	969.9	20.1	
38.1	11.2	769.9	16.0	
50.8	12.3	350.0	7.3	
63.5	15.1	230.0	4.8	
76.2	18.2	190.0	3.9	
88.9	21.7	140.0	2.9	
<b>Sample ID:</b>		<b>Thickness, b (mm):</b>	<b>Displacement Rate, <math>\Delta^*</math> (mm/min) :</b>	
<b>SWR06T</b>		<b>45.47</b>	<b>0.889</b>	
12.7	5.0	1049.9	23.1	<b>10.945</b>
25.4	6.6	739.9	16.3	
38.1	8.7	629.9	13.9	
50.8	10.8	440.0	9.7	
63.5	11.6	330.0	7.3	
76.2	14.3	260.0	5.7	
88.9	17.5	140.0	3.1	

Table 13 Summary of Test Results for the Asphalt Rubber Gap Mix.

Crack Length, a (mm)	Time T, (Min)	Force, P (N)	Force per Unit Thickness P* (N/mm)	Crack Growth Rate, a* (mm/min)
<b>Sample ID:</b>		<b>Thickness, b (mm):</b>	<b>Displacement Rate, Δ* (mm/min) :</b>	
<b>SWG04B</b>		<b>46.48</b>	<b>0.381</b>	
12.7	9.7	850.0	18.3	<b>5.463</b>
25.4	16.3	550.0	11.8	
38.1	18.3	495.0	10.6	
50.8	19.3	450.0	9.7	
63.5	23.4	320.0	6.9	
76.2	27.2	260.0	5.6	
88.9	41.8	100.0	2.2	
<b>Sample ID:</b>		<b>Thickness, b (mm):</b>	<b>Displacement Rate, Δ* (mm/min) :</b>	
<b>SWG04M</b>		<b>45.97</b>	<b>0.508</b>	
12.7	9.7	1009.2	22.0	<b>6.662</b>
25.4	7.9	919.3	20.0	
38.1	10.0	819.3	17.8	
50.8	12.5	599.5	13.0	
63.5	14.0	449.6	9.8	
76.2	18.8	339.7	7.4	
88.9	33.0	88.9	1.9	
<b>Sample ID:</b>		<b>Thickness, b (mm):</b>	<b>Displacement Rate, Δ* (mm/min) :</b>	
<b>SWG04T</b>		<b>45.72</b>	<b>0.635</b>	
12.7	6.5	1109.9	24.3	<b>7.150</b>
25.4	7.6	1089.9	23.8	
38.1	10.2	699.9	15.3	
50.8	11.8	530.0	11.6	
63.5	14.7	360.0	7.9	
76.2	17.8	220.0	4.8	
88.9	26.3	85.0	1.9	
<b>Sample ID:</b>		<b>Thickness, b (mm):</b>	<b>Displacement Rate, Δ* (mm/min) :</b>	
<b>SWG05M</b>		<b>46.99</b>	<b>0.762</b>	
12.7	7.1	1379.9	29.4	<b>7.874</b>
25.4	9.6	1019.9	21.7	
38.1	11.2	769.9	16.4	
50.8	12.3	589.9	12.6	
63.5	15.1	380.0	8.1	
76.2	18.2	150.0	3.2	
88.9	21.7	110.0	2.3	
<b>Sample ID:</b>		<b>Thickness, b (mm):</b>	<b>Displacement Rate, Δ* (mm/min) :</b>	
<b>SWG05T</b>		<b>45.21</b>	<b>0.889</b>	
12.7	5.0	1439.9	31.8	<b>5.939</b>
25.4	6.6	1189.9	26.3	
38.1	8.7	859.9	19.0	
50.8	10.8	619.9	13.7	
63.5	11.6	440.0	9.7	
76.2	14.3	240.0	5.3	
88.9	17.5	100.0	2.2	

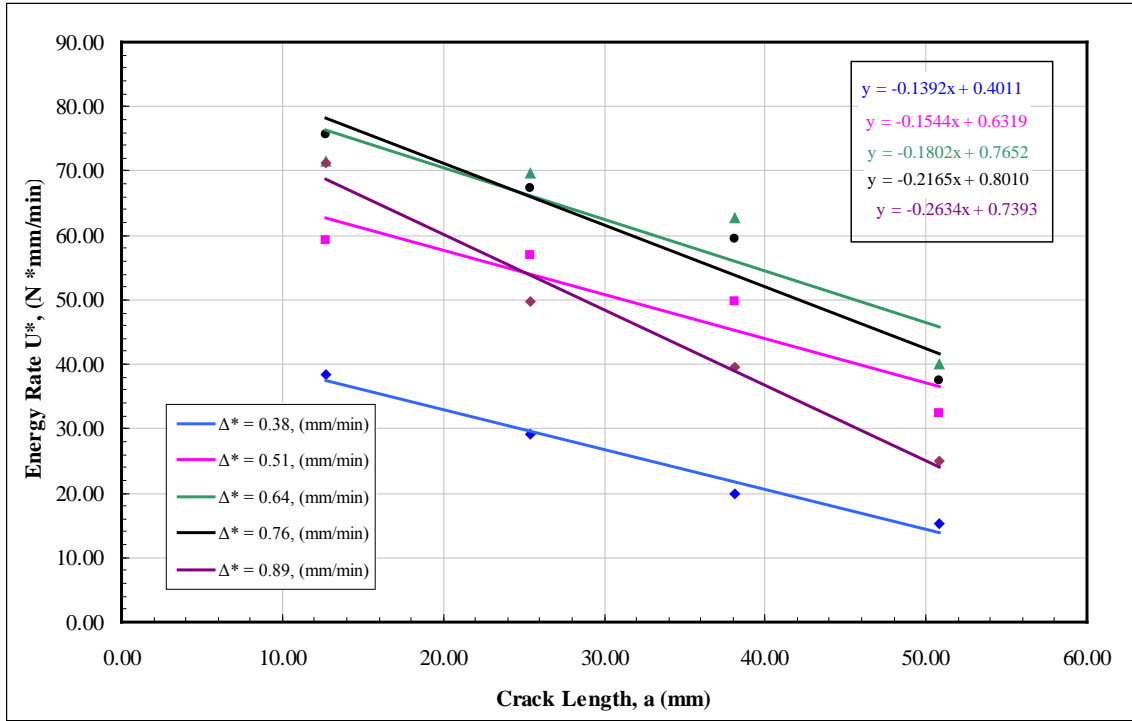


Figure 28 Crack Lengths versus Energy Rate for the Reference Gap Mix.

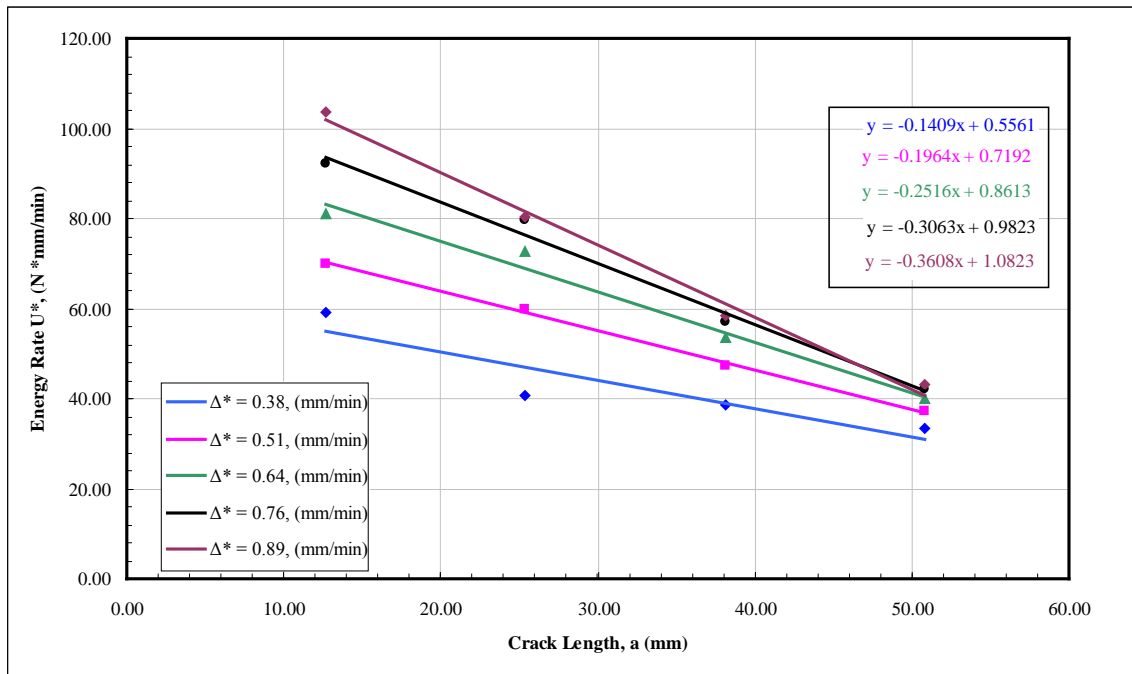


Figure 29 Crack Lengths versus Energy Rate for Asphalt Rubber Gap Mix.

Figure 30 shows relationships between crack growth rates and  $C^*$  values for the two mixtures. It is observed that the asphalt rubber gap graded mix has about 4 times higher slope value when compared to the reference gap graded mix. This is an indication that the asphalt rubber gap graded mix has higher resistance to crack propagation. It is also indicative that more energy is required for the asphalt rubber mix to develop full depth cracks compared to the reference mix.

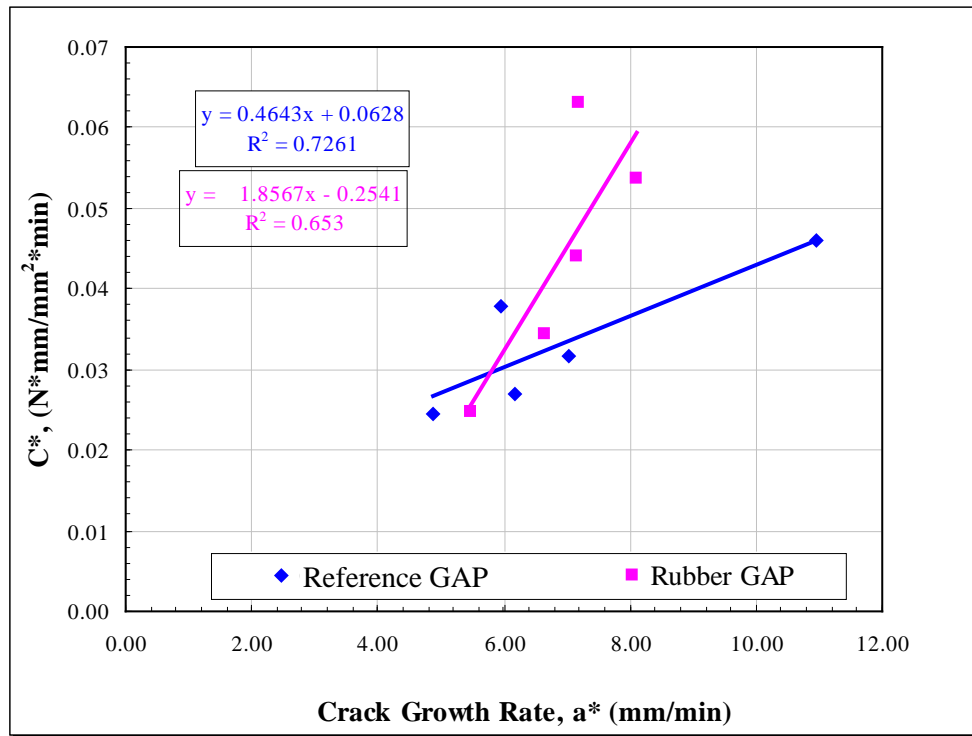


Figure 30 Crack Growth Rate versus  $C^*$  Values For Reference and Rubber Gap Mixes.

## **7. TIRE / ROAD NOISE LABORATORY EVALUATION**

Analyses were performed on laboratory  $E^*$  test results of both mixtures. Specifically, the phase angle from the  $E^*$  test was the parameter of interest. As explained earlier,  $E^*$  tests were performed on all the samples to obtain phase angle,  $\phi$  at five temperatures (-10, 4.4, 21.1, 37.8 and 54.4 °C) and six different frequencies (25, 10, 5, 1, 0.5 and 0.1 Hz). The phase angle indicates the amount of viscous and/or elastic response of the material being evaluated. A viscous material would dampen noise more than an elastic one. Figure 31 shows an asphalt mixture stress-strain response under sinusoidal load for different levels of viscoelastic behavior.

Figure 31 Asphalt Mixture Stress-Strain Responses under Sinusoidal Load for Different Levels of Viscoelastic Behavior

## 7.1. Phase Angle Test Results

Table 14 presents results of average phase angles (three replicates each) for the reference as well as asphalt rubber gap graded mixtures at the five test temperatures and six frequencies. The results indicate that the phase angles of reference gap graded mixture are slightly higher (or closer at certain temperatures and frequencies) than those for the asphalt rubber gap graded mixture.

Table 14 Phase Angle Test Results of Swedish Gap Graded Mixtures

Temperature (°C)	Frequency (Hz)	Reference Gap Graded	Asphalt Rubber Gap Graded
-10	25	3.7	8.0
-10	10	6.5	9.5
-10	5	7.6	10.7
-10	1	9.7	11.3
-10	0.5	10.4	12.5
-10	0.1	13.8	14.3
4.4	25	11.0	11.8
4.4	10	16.0	15.9
4.4	5	19.0	16.8
4.4	1	24.9	22.0
4.4	0.5	28.6	24.6
4.4	0.1	36.6	30.0
21.1	25	27.2	22.6
21.1	10	31.8	28.5
21.1	5	34.4	29.3
21.1	1	39.6	35.0
21.1	0.5	40.5	36.7
21.1	0.1	40.2	39.2
37.8	25	36.2	31.7
37.8	10	36.4	33.6
37.8	5	34.9	32.5
37.8	1	31.5	33.0
37.8	0.5	28.8	32.6
37.8	0.1	25.7	31.3
54.4	25	33.4	35.8
54.4	10	27.9	32.2
54.4	5	25.7	30.9
54.4	1	23.0	26.6
54.4	0.5	22.7	24.5
54.4	0.1	22.6	19.8

## 7.2. Phase Angle Master Curve

Understanding viscoelastic properties of HMA mix is dependent on both times of loading and temperature. This special characteristic makes the characterization of an asphalt mixture a very complex problem. This problem can be reduced by the use of time-temperature superposition. In this direction, the construction of a master curve for the phase angle ( $\phi$ ) of a specific mix, is constructed at a reference temperature (generally taken as 21.1 °C). The phase angle data at other temperatures are shifted with respect to time (or frequency) until the curves merge into single smooth function. The master curve of the phase angle, as a function of time (or frequency), formed in this manner describes the time dependency of the material.

Figure 32 presents master curves for the reference and asphalt rubber gap graded mixtures. It can be observed that the peak phase angle for the reference gap graded mixture is about 2° higher than the peak of the asphalt rubber gap graded mixture. Peak of the phase angle represents the maximum noise-dampening potential of the pavement material. These results seem to be very rational especially when compared with the field noise level measurements (provided by Swedish Transport Institute, VTI). Table 15 provides such relationships between laboratory measured phase angle and field noise measurements for 5 Hz test frequency (~50 km/h) and 10 Hz (~80 km/h). The higher the phase angle, the lower is the field noise.

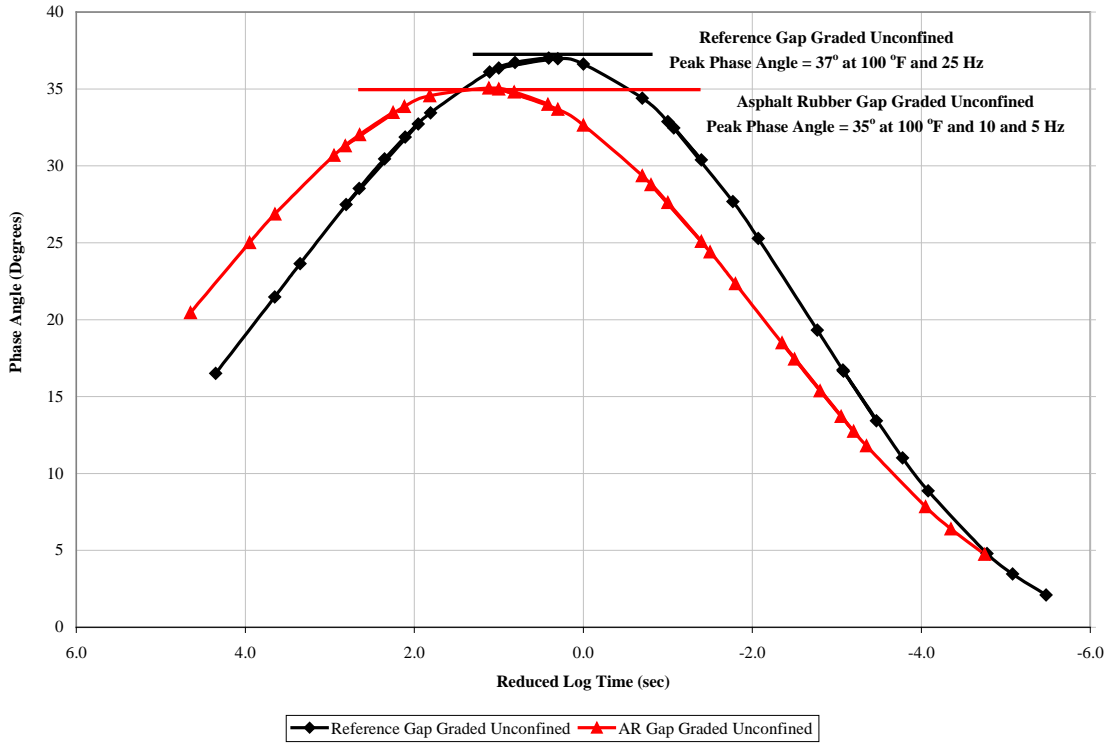


Figure 32 Phase Angle Master Curves for the Reference and Asphalt Rubber Gap Graded Mixtures.

Table 15 Relationship between Phase Angle and Field Noise for Different Vehicle Speeds

No.	Surface Name	Representing light vehicles Tyres CPXA & SRTT			
		Speed [km/h]			
		50		80	
		Noise (dB)	Phase Angle (deg)	Noise (dB)	Phase Angle (deg)
AR 0 (Reference Gap Graded)	SMA 0/16 (reference)	94.22	34.4	100.92	31.8
AR 1 (Asphalt Rubber Gap Graded)	SMA 0/16 w rubber	94.35	29.3	101.14	28.5

## **8. SUMMARY AND CONCLUSIONS**

### **8.1. Summary**

A reference gap graded asphalt mix along with an asphalt rubber gap graded mixture was sampled during construction from pavement test sections by the Swedish Road Administration, Sweden. The mixtures were placed on Malmo E6 External Ring Road. The mixtures were sent to Arizona State University (ASU) laboratories for testing and evaluation. At ASU, laboratory test specimen preparation included compaction of 150 mm diameter gyratory specimens for triaxial testing, and beam specimens prepared and compacted according to AASHTO TP8 test protocols. The target air void level for the test specimens were those reported in the field (about 2%). Rice gravities were determined for the loose mixtures, as well as thickness and bulk densities measured in preparation of the testing program.

The advanced material characterization tests included: Dynamic (Complex) Modulus for stiffness evaluation, Flexural Beam test for fatigue cracking evaluation, and C\* Integral test to evaluate crack growth and propagation.

### **8.2. Conclusions**

#### **8.2.1. Dynamic (Complex) Modulus E\* Test**

The AASHTO TP 62-03 Test Method was followed for E\* testing. For each mix, three replicates were prepared for testing. For each specimen, E\* tests were conducted at -10, 4.4, 21.1, 37.8 and 54.4 °C for 25, 10, 5, 1, 0.5 and 0.1 Hz loading frequencies. E\* master curves of all mixtures were constructed for a reference temperature of 21.1 °C using the principle of

time-temperature superposition. The Reference gap graded mixture showed higher moduli values at lower temperatures (-10 and 4.4 °C) while the trend was reversed with further increase in temperature to 54.4 °C. This indicated that the asphalt rubber gap graded mix would provide better resistance low temperature cracking (softer modulus at lower temperatures) and to permanent deformation (stiffer modulus at higher temperatures).

### **8.2.2. Repeated Load Permanent Deformation Flow Number Test**

The repeated load permanent deformation flow number tests were conducted unconfined at 30 °C and at a stress level of 1,034 kPa (150 psi). The average FN of the AR-Gap graded mixtures were about 5.5 times higher than the Reference-Gap graded mixtures; thus, the AR-Gap graded mixtures are anticipated to be less susceptible to permanent deformation.

### **8.2.3. Fatigue Cracking Test**

Constant strain Flexural tests were performed according to the AASHTO TP8 and SHRP M-009 procedures to evaluate the fatigue performance of both mixtures. Based on the test results and analyses, the following conclusions are made:

- The generalized fatigue models developed show excellent measures of accuracy for both the reference and asphalt rubber gap graded mixtures.
- Comparing the initial stiffness for both mixtures at 21.1 °C, it was observed that the asphalt rubber gap graded mixture shows lower stiffness values compared to the reference mixture.
- At lower strain values, the fatigue life was higher for the asphalt rubber gap graded mixture; while at higher strain values the fatigue life is higher for reference gap

graded mixture. Since the pavement sections are part of a highway, the expected fatigue life for the AR gap graded mixture is higher than the reference mix as the strain level conditions are anticipated to be lower (~80 km/h vehicle speed). If the same two mixtures are used on roads with lower design speeds (such as parking lots and intersections), it is anticipated that the reference mixture will provide higher fatigue life than the AR gap graded mixture.

#### **8.2.4. Crack Propagation Test – C\* Integral**

Relationships between crack growth rates and C\* Line Integral values for both mixtures were presented. It was observed that the asphalt rubber gap graded mix has about 4 times higher slope value when compared to the reference gap graded mix. This is an indication that the asphalt rubber gap graded mix has higher resistance to crack propagation. It is also indicative that more energy is required for the asphalt rubber mix to develop full depth cracks compared to the reference mix.

#### **8.2.5. Laboratory Pavement / Tire Noise Evaluation Using Phase Angle Test Results**

The peak phase angle for the reference gap graded mixture was found to be about 2° higher than the peak of the asphalt rubber gap graded mixture. Peak of the phase angle represents the maximum noise-dampening potential of the pavement material. These results seemed to be rational especially when compared with the field noise level measurements (provided by Swedish Transport Institute, VTI). The higher the phase angle, the lower is the field noise.

## REFERENCES

1. SHRP Designation: M-009. Standard Method of Test for Determining the Fatigue Life of Compacted Bituminous Mixtures Subjected to Repeated Flexural Bending.
2. AASHTO Designation: T321-03. Determining the Fatigue Life of Compacted Hot-Mix Asphalt (HMA) Subjected to Repeated Flexural Bending.
3. Witczak, M. W., Kaloush, K. E., Pellinen, T., El-Basyouny, M., & Von Quintus, H. Simple Performance Test for Superpave Mix Design. NCHRP Report 465. Transportation Research Board. National Research Council. Washington D.C. 2002.
4. SHRP-A-404. *Fatigue Response of Asphalt-Aggregate Mixes*. Asphalt Research Program, Institute Of Transportation Studies, University Of California, Berkeley. Strategic Highway Research Program, National Research Council, Washington, D.C., 1994.
5. AASHTO Designation: T321-03. Determining the Fatigue Life of Compacted Hot-Mix Asphalt (HMA) Subjected to Repeated Flexural Bending.
6. SHRP Designation: M-009. Standard Method of Test for Determining the Fatigue Life of Compacted Bituminous Mixtures Subjected to Repeated Flexural Bending.
7. Witczak, M.W., Mamlouk, M., and Abojaradeh, M. *Flexural Fatigue Tests*. NCHRP 9-19, Subtask F6 Evaluation Tests. Task F Advanced Mixture Characterization. Interim Report, Arizona State University, Tempe, Arizona, July 2001.

8. Harvey, J., and Monismith, C.L., Effect of Laboratory Asphalt Concrete specimen Preparation Variables on Fatigue and Permanent Deformation Test Results Using Strategic Highway Research Program A-003A Proposed Testing Equipment. Record 1417, Transportation Research Board, Washington, D.C., 1993.
9. Tayebali, A. A., Deacon, J. A., and Monismith, C. L., Development and Evaluation of Surrogate Fatigue Models for SHRP. A-003A Abridged Mix Design Procedure. Journal of the Association of Asphalt Paving Technologists Vol. 64, 1995, pp. 340-366.
10. S. J. Sulaiman and A. F. Stock, "The Use of Fracture Mechanism for the Evaluation of Asphalt Mixes", AAPT, V64., 1995.
11. M. Mamlouk and B. Mobasher, "Cracking Resistance of Asphalt Rubber Mix Versus Hot-Mix Asphalt", International Journal of Road Materials and Pavement Design. V.5., 4, pp. 435-452., 2004.
12. Majidzadeh, K., et al., "Application of Fracture Mechanics for Improved Design of Bituminous Concrete," Volumes 1 and 2, Report FHWA-RD-76-91, Federal Highway Administration, Washington, D.C., 1976.
13. Abdulshafi, O., "Rational Material Characterization of Asphaltic Concrete Pavements," Ph.D. Dissertation, the Ohio State University, Columbus, OH, 1983.
14. Rice. J. R., Journal of Applied Mechanics, American Society of Mechanical Engineers, Volume 35, pp. 379-386., 1968.

15. Begley, J. W. and Landes, J. D., Fracture Toughness, Processing of the 1971 National Symposium on Fracture Mechanics. Part II, ASTM STP 514, American Society for Testing Materials pp. 1-20., 1972.
16. Abdulshafi, A. and K.E. Kaloush. "Modifiers for Asphalt Concrete." ESL-TR-88-29, Air Force Engineering and Services Center, Tyndall Air Force Base, Florida, 1988.
17. Method for Preparation of Triaxial Specimens (Test Protocol UMD 9808), "Superpave Models Team Inter-Laboratory Testing Manual." University of Maryland, College Park, MD, 1998.